Remote Sensing of Environment 136 (2013) 416–432

Contents lists available at SciVerse ScienceDirect

Remote Sensing of Environment

journal homepage: www.elsevier.com/locate/rse

Bio-optical characteristics of the Patagonia Shelf break waters: Implications for ocean color algorithms

Amabile Ferreira [a,*], Carlos A.E. Garcia [a], Ana I. Dogliotti [b], Virginia M.T. Garcia [a]

[a] Instituto de Oceanografia, Universidade Federal do Rio Grande — FURG, Av. Itália, Km 8, 96201-900 Rio Grande, Brazil
[b] Instituto de Astronomía y Física del Espacio (IAFE-CONICET), Ciudad Universitaria, Casilla de Correo 67-Suc. 28 (C1428ZAA), Ciudad Autónoma de Buenos Aires, Argentina

ARTICLE INFO

Article history:
Received 27 November 2012
Received in revised form 2 May 2013
Accepted 20 May 2013
Available online 22 June 2013

Keywords:
Phytoplankton
Absorption
Scattering
Remote sensing reflectance
Patagonia

ABSTRACT

Bio-optical data for spring and summer phytoplankton blooms at 176 stations along the Patagonia Shelf break and adjacent areas were collected from October 2006 to January 2009 during six cruises. Data included chlorophyll-*a* concentration (Chl*a*), coefficients of particulate absorption, $a_p(\lambda)$, phytoplankton absorption, $a_{ph}(\lambda)$, beam attenuation, $c_p(660)$, diffuse attenuation, $K_d(\lambda)$, and hyperspectral remote sensing reflectance, $R_{rs}(\lambda)$. Surface Chl*a* varied within a wide range from 0.10 to 18.87 mg m^{-3} (mean of 2.82 ± 3.35), reflecting differences in both the timing of the blooms and the geographical sampling area. Considerable dispersion was verified for $a_p(\lambda)$, $c_p(660)$, and $K_{bio}(440)$ ($K_d(440)$ minus diffuse attenuation for pure water) as a function of Chl*a*. A hierarchical cluster analysis (HCA) applied to the $R_{rs}(\lambda)$ spectra ($N = 116$) resulted in three classes ordered by spectral features that varied according to Chl*a*. Class 1 ($N = 22$), Class 2 ($N = 52$), and Class 3 ($N = 42$) were grouped according to the $R_{rs}(\lambda)$ associated with Chl*a* average of 0.86 (±0.51), 2.42 (±1.62), and 8.40 mg m^{-3} (±3.96), respectively. The estimation of Chl*a* and $a_{ph}(\lambda)$ by empirical and semi-analytical algorithms was evaluated using satellite data. Errors in the Chl*a* estimates from the empirical algorithm OC4v6 using in situ $R_{rs}(\lambda)$ showed significant statistical relationships with Chl*a*, $a_{ph}(440)$ / Chl*a*, and $b_p(660)$ / Chl*a* (where $b_p(660) = c_p(660) - a_p(660)$). Although reasonable agreements were found between the measured and satellite-estimated values, the dependence of the OC4v6 errors on the Chl*a*-specific phytoplankton absorption and particulate scattering coefficients reinforces the need to regionally refine both empirical and semi-analytical algorithms to improve satellite estimates of the bio-optical variables for the Patagonia region.

1. Introduction

At present, several bio-optical studies seek to reduce the oversimplification associated with models of optical properties that use chlorophyll-*a* concentration as a proxy for phytoplankton and related water constituents (Arnone et al., 2004; Mobley et al., 2004); however, the classical bio-optical classification of waters as Case 1 or 2 is still useful for modeling purposes. In Case 1 waters, phytoplankton and their accompanying retinue of dissolved and particulate biological material govern the water's bio-optical properties. The opposite is true of Case 2 waters, which are significantly influenced by non-algal constituents, including mineral particles, Colored Dissolved Organic Matter (CDOM), microbubbles, the concentrations of which do not vary with the phytoplankton concentration (Morel & Prieur, 1977).

Apparent and inherent optical properties, AOP and IOP, respectively (sensu Preisendorfer, 1961), have been widely analyzed for Case 1 waters and are empirically correlated with chlorophyll-*a* concentration (Chl*a*). Indeed, the relationship between IOP and Chl*a* shows robust general trends over orders of magnitudes (e.g., Morel, 1988; Morel & Maritorena, 2001; Morel et al., 2007). For a given Chl*a*, variations in the AOP and IOP is expected because of possible fluctuations in (1) the pigment composition and packaging effects within the phytoplankton assemblages, (2) the proportion of algal and non-algal particles, and (3) the proportion of particulate matter (algal plus non-algal) and CDOM. In high-Chl*a* Case 1 waters, bio-optical properties could be even influenced by the age and nutrient status of the algal population (Morel et al., 2006). Furthermore, due to lack of data for eutrophic waters, the empirical relationships between Chl*a* and AOP or IOP seem to be less robust and noisier then in oligotrophic regions (O'Reilly et al., 1998). In order to address the question of whether there is a greater bio-optical variability in high-Chl*a* (Case 1) waters, the analysis of a more diversified dataset is required including data from upwelling zones (Morel et al., 2006).

In general, phytoplankton absorption properties have been well characterized through laboratory and field measurements. The relationship between the phytoplankton absorption and Chl*a* has shown high variability (e.g., Bricaud et al., 1995; Dmitriev et al., 2009). Based on a large dataset, Bricaud et al. (2004) examined the causes of phytoplankton absorption variability by explicitly separating the impact of changes in pigment composition from changes in pigment packaging, which are due to intracellular pigment concentrations and variations in cell size

* Corresponding author. Tel.: +55 1281861016.
E-mail address: amabilefr@gmail.com (A. Ferreira).

0034-4257/$ – see front matter © 2013 Elsevier Inc. All rights reserved.
http://dx.doi.org/10.1016/j.rse.2013.05.022

(Kirk, 1975). The variation around the mean was systematic rather than random and primarily resulted from variability in the packaging effect associated with variations in the size structure of the algal community, even within a given geographical area. This could be attributed to both regional and seasonal changes in the phytoplankton communities. Several approaches involving both in situ and satellite remote sensing of phytoplankton absorption coefficients have been used to derive size structure of algal communities (e.g., Aiken et al., 2006; Brewin et al., 2010; Ciotti & Bricaud, 2006; Ciotti et al., 2002; Hirata et al., 2008).

Empirical relationships using field data have related Chl*a* to the beam attenuation coefficient (e.g., Loisel & Morel, 1998; Voss, 1992), the scattering coefficient (Loisel & Morel, 1998), and the backscattering coefficient (Huot et al., 2008; Martinez-Vicente et al., 2010; Stramska et al., 2006). Irrespective of the variability found in those relationships among different studies, Behrenfeld and Boss (2006) noted that the beam attenuation at 660 nm, $c_p(660)$, may be used as a viable index of phytoplankton carbon biomass in ecosystems where phytoplankton biomass and $c_p(660)$ are temporally stable and also as a phytoplankton physiological index in changing growth conditions (Behrenfeld & Boss, 2003). Recently, Westberry et al. (2010) argued that both phytoplankton biomass and physiological indices can be conceptually assessed by analyzing the relationships between either $c_p(\lambda)$ or Chl*a*:$c_p(\lambda)$ and the particulate backscattering coefficient, $b_{bp}(\lambda)$.

Satellite estimates of Chl*a* have been extensively based on empirical algorithms derived from statistical relationships between Chl*a* and the normalized water leaving radiance, $L_{wn}(\lambda)$, or remote sensing reflectance, $R_{rs}(\lambda)$ (the ratio of water leaving radiance to downwelled irradiance), such as the OC4v6 model currently used to estimate Chl*a* from the Sea-viewing Wide Field-of-view Sensor (SeaWiFS) data (O'Reilly et al., 1998, updated in http://oceancolor.gsfc.nasa.gov/REPROCESSING/R2009/ocv6/). However, a new empirical approach that reduces the bias of ocean chlorophyll estimates has been recently developed (Gregg et al., 2009).

$R_{rs}(\lambda)$ is not solely dependent on phytoplankton biomass (indexed as Chl*a*) but is directly proportional to the ratio of backscattering and absorption coefficients for all components in the water, $b_b(\lambda)$ / $a(\lambda)$, including the scattering and absorption of the water itself. Understanding the processes that cause changes in the spectral behavior of the optical components and quantifying the variability of their IOP should improve the retrieval accuracy of individual parameters using remote-sensing techniques (IOCCG, 2006; Lee et al., 2010). For instance, although IOP-based algorithms are comparable in performance to the standard empirical chlorophyll algorithms, the semi-analytical models also allow studies of chlorophyll biomass variability as a function of phytoplankton and CDOM absorption (Szeto et al., 2011 and references therein). Brown et al. (2008) have quantified the impact of optical anomalies on the ocean color signal based on their optical sources (absorption and backscattering coefficients). The authors have identified two sources of secondary variability: 1) the amount of non-algal absorption, especially due to CDOM and 2) the amplitude of the particle backscattering coefficient.

During the austral spring and summer, satellite ocean color images have revealed that high levels of phytoplankton biomass persistently occur in the Patagonia inner shelf and shelf break region, which is considered one of the most globally productive ocean zones. The seasonal cycle of phytoplankton biomass in the vicinity of the Patagonia Shelf break front has been well described by remote sensing in recent years (Garcia et al., 2004; Rivas et al., 2006; Romero et al., 2006; Signorini et al., 2006).

The development and maintenance of these phytoplankton blooms are associated with nutrient supply from Malvinas Current and the water column stability along the shelf-break front (Garcia et al., 2008). In fact, upwelling process at that front (Matano & Palma, 2008) also contributes with deep nutrient supply for phytoplankton growth. The Argentinean continental shelf has been recognized as a relevant region in terms of standing stocks of primary producers and contribution to the global primary production (e.g., Gregg et al., 2005). High primary productivity rates (1.9 to 7.8 mg C m^{-2} d^{-1}) were measured in the area during spring (Garcia et al., 2008) and the variability in photosynthetic parameters was shown to be associated with the light absorption properties of the phytoplankton composition (Lutz et al., 2010). Specifically, Ferreira et al. (2009) described an important difference in phytoplankton absorption coefficients between spring and late summer periods that was attributed to differences in the phytoplankton size structure.

The observed seasonality of phytoplankton aspects (composition, light absorption, and photosynthetic parameters) has an important implication for the regional ecology and carbon cycle, because the efficiency of energy transfer throughout the trophic levels is related to the phytoplankton cell size (Guidi et al., 2010; Kiørboe, 1993), and the CO_2 uptake by seawater is influenced by the phytoplankton composition (Bopp et al., 2005; see revision by Le Quéré et al., 2005). For instance, studies in the Argentinean continental shelf have shown that when phytoplankton assemblages were dominated by large diatoms, both phytoplankton biomass (Chl*a*) and net community production were inversely proportional to ΔpCO_2 and directly related to % O_2 saturation (Schloss et al., 2007). This was not the case when small ($\leq$5 μm) flagellates dominated. The region makes an important contribution to the global oceanic CO_2 uptake from the atmosphere (Bianchi et al., 2009).

Despite the ecological and biogeochemical relevance of the Patagonia Shelf, in situ bio-optical measurements (IOP and AOP properties) are scarce in the region and the lack of a comprehensive bio-optical study is a major obstacle for better estimates of ocean color products such as Chl*a*. Regional particularities in the optical properties of the Patagonia waters might impact the performance of bio-optical algorithms. Moreover, there is a lack of specific analyses of the performance of existing algorithms for the region's satellite data. Dogliotti et al. (2009) reported that NASA's operational algorithms generally overestimates at low Chl*a* (<1 mg m^{-3}) and underestimates at high Chl*a* (>1 mg m^{-3}). This was attributed to the lack of bio-optical measurements at high pigment concentrations when the algorithm was generated in the late 1990s (O'Reilly et al., 1998, 2000).

The Patagonia experiment (PATEX) is a research project conducted under the Brazilian Antarctic Program. Within the project objectives are the characterization of the phytoplankton assemblages, bio-optical properties, and primary production rates of the waters along the Argentinean Shelf break and the environmental constraints associated with the blooms during spring and summer. Seven cruises were conducted between 2004 and 2009 in the Argentinean Patagonia Shelf break and adjacent areas. In this study, we present results of the bio-optical data from six cruises carried out in the region during spring and summer phytoplankton blooms.

The present work aims to investigate the relationships between Chl*a* and IOP (particulate absorption and attenuation coefficients) and AOP (diffuse attenuation coefficient) within the phytoplankton blooms in the Patagonia waters, contributing with data on bio-optical properties of high-Chl*a* waters (Morel et al., 2006). We also describe the variability in the spectra of hyperspectral remote sensing reflectance and evaluate the retrieval of Chl*a* and phytoplankton absorption coefficients through current empirical and semi-analytical algorithms using both in situ and satellite reflectance data. In addition, we investigate the relationship between the variations in absorption and scattering coefficients normalized by Chl*a* and the errors associated with Chl*a* estimates from empirical algorithms.

2. Material and methods

2.1. Oceanographic cruises and sections

The Patagonia Shelf break and a portion of the inner shelf were extensively sampled (176 stations) by performing cross- and along-shelf transects during the PATEX cruises in the austral spring (October 2006, 2007,

and 2008 and PATEX 2, 4 and 6, respectively) and summer (March 2007, January 2008 and 2009 and PATEX 3, 5 and 7, respectively). The geographical positions of the sampling stations (Fig. 1) spanned from the northern portion of the Argentinean Shelf (PATEX 6) through the highly productive waters along both the Patagonia Shelf break (PATEX 2 to 4) and the southern inner shelf (PATEX 5) to the southern end of the Malvinas (Falkland) Islands (PATEX 7).

The following measurements were made at all the 176 stations: (i) total Chl*a*, (ii) particulate (phytoplankton and detritus) absorption, and (iii) beam attenuation coefficient at 660 nm. The (iv) diffuse attenuation coefficient and (v) hyperspectral remote sensing reflectance were measured at 116 stations during daylight hours and are indicated in Fig. 1 as filled markers.

2.2. Chlorophyll-a concentration

Discrete samples for Chl*a* were collected at the surface and selected depths along the water column ($N = 790$) based on the chlorophyll fluorescence profile and filtered onto 25 mm glass fiber filters (Whatman® GF/F). After filtration, the filters were wrapped in aluminum foil and transferred to liquid nitrogen for later analysis. At the laboratory, the pigment was extracted in 90% acetone and the fluorescence was determined with a Turner Designs TD-700 fluorometer (previously calibrated with Sigma® chlorophyll-*a* standard) following the non-acidification method from Welschmeyer (1994).

2.3. Particulate absorption coefficient

The spectra of the particulate absorption coefficient, $a_p(\lambda)$ in m^{-1}, were obtained with the quantitative filter pad technique (Kishino et al., 1985) using water samples (0.5–2 L) collected at the surface, the depths of maximum chlorophyll fluorescence (MCF), and bottom of the peak of chlorophyll fluorescence (BMCF) ($N = 356$). These samples were filtered onto 25-mm Whatman GF/F filters. Immediately after filtration, the GF/F filters were wrapped in aluminum foil and placed in liquid nitrogen for storage. The $a_p(\lambda)$ measurements were made in the 300–750 nm spectral range at 1-nm intervals with a dual beam spectrophotometer (Cary Model 1E). Immediately after the $a_p(\lambda)$ measurements, the sample filters were subjected to methanol extraction (for the PATEX 2 and 3 cruises) and bleaching with sodium hypochlorite (PATEX 4, 5, 6 and 7 cruises) and then re-scanned to obtain estimates of the non-algal particle (detritus) absorption coefficient, $a_d(\lambda)$ (Kishino et al., 1985; Mitchell et al., 2000; Tassan & Ferrari, 1995). The bleaching method was applied in the last cruises because of its advantages over the extraction method, as it is faster and more efficient in bleaching water-soluble pigments (Tassan & Ferrari, 1995). Since the contribution of cyanobacteria (the main water-soluble pigments containing species) is very low in our samples (M. Souza, personal communication), any difference in phytoplankton absorption between cruises is unlikely to be due to different methods of pigments extraction. For the calculations of the $a_p(\lambda)$ and $a_d(\lambda)$ coefficients, the amplification factor β given by Ferreira et al. (2009) was used. The spectral absorption coefficient of phytoplankton, $a_{ph}(\lambda)$, was calculated as the difference between $a_p(\lambda)$ and $a_d(\lambda)$.

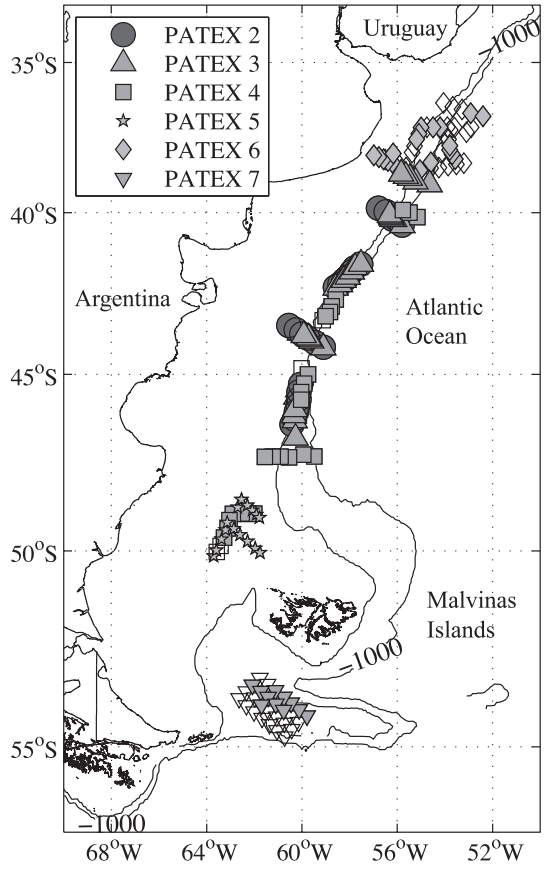

Fig. 1. Locations of the 176 oceanographic stations where measurements and sample collections were taken during the PATEX cruises along the Patagonian Shelf break and adjacent areas. Filled symbols indicate the stations where data collection was carried out during the daylight hours and $K_d(\lambda)$ and $R_{rs}(\lambda)$ data are available.

2.4. Particulate attenuation coefficient

The beam attenuation coefficient of suspended particles at 660 nm, $c_p(660)$ in m^{-1}, was measured with a C-star beam transmissometer (WETLabs, Inc.) along a 25-cm pathlength through the water column. In this study, we used 790 measurements of $c_p(660)$, matching the number of Chl*a* data. Details of the protocol for determining $c_p(660)$ are provided by the manufacturer of the C-star beam transmissometer (http://www.wetlabs.com/cstar). We assumed that measurements taken in deep waters (~1000 m) but still far away from the sea bottom provided the best estimate of particle-free attenuation of the seawater (Loisel & Morel, 1998). These deep-water measurements were subtracted from all beam attenuation measurements taken at the surface ocean layer on a cruise-by-cruise basis to remove the contribution of pure seawater. The resulting values represent the beam attenuation by particles, assuming that the contribution of dissolved matter to the attenuation of light at 660 nm is negligible. We also note that the measurements taken at 5 m depth were assumed to represent the near-surface beam attenuation, which is reasonable given that it avoids or minimizes the potential intermittent contributions of air bubbles injected by breaking waves.

2.5. Hyperspectral diffuse attenuation coefficient and remote sensing reflectance

Underwater radiometric measurements were obtained at stations during daylight hours ($N = 116$) with a hyperspectral profiling radiometer (HyperOCR, Satlantic, Inc.), which measures the upwelling radiance, $L_u(\lambda,z)$, and the downward irradiance, $E_d(\lambda,z)$, over the 350–800 nm spectral range with a resolution of 3.3 nm (137 spectral bands). The spectral remote sensing reflectance, $R_{rs}(\lambda)$ in sr^{-1}, is defined as the ratio of nadir water-leaving radiance, $L_w(\lambda)$, to the downwelling plane irradiance, $E_d(\lambda)$, just above the sea surface (0^+). The measured $L_u(\lambda,z)$ and $E_d(\lambda,z)$ in the water column are used to estimate their values just beneath the surface, $L_u(\lambda, 0^-)$ and $E_d(\lambda, 0^-)$, and then are propagated through to the sea–air interface to obtain $L_w(\lambda)$ and $E_d(\lambda,0^+)$.

The initial data processing was performed using ProSoft ver. 7.7.11 processing software, developed and distributed by Satlantic Inc. Dark offsets and the manufacturer's radiometric calibrations were applied to the raw data, and the spectral radiometric data were binned

every 0.1 m. Because of surface waves, it was rarely possible to measure $E_d(\lambda,z)$ and $L_u(\lambda,z)$ closer to the sea surface. The shallowest reliable readings typically occurred at depths ranging from 0.5–2 m. The data from this zone usually exhibited strong fluctuations associated with surface waves, and thus it was necessary to extrapolate the data upward to the sea surface. Matlab® routines were developed to analyze each radiometric profile and process the radiometric data. Visualization of E_d (λ,z), L_u (λ,z), *PAR* (photosynthetic available radiance) percentage, and tilt angle were used to analyze the quality of each profile and the depth interval to be used to extrapolate the values to just below the water surface.

The diffuse attenuation coefficients of downwelling irradiance, $K_d(\lambda)$, and upwelling radiance, $K_u(\lambda)$, were calculated as the slope of a least-squares linear regression of the log-transformed $E_d(\lambda,z)$ and $L_u(\lambda,z)$, respectively, within the selected depth interval, which generally ranged between 2 to 7 m. Using these coefficients, $L_u(\lambda,z)$ and $E_d(\lambda,z)$ were propagated to just below the water surface by fitting an exponential function to the profile data. The remote sensing reflectance was then calculated using the following equation: $R_{rs}(\lambda) = 0.54\ L_u(\lambda,0^-) / (1.04\ E_d(\lambda,0^-))$, where 0.54 and 1.04 are the transfer coefficients of the air–sea interface for $L_u(\lambda)$ and $E_d(\lambda)$, respectively (Austin, 1974). The fraction of $K_d(\lambda)$ associated with the presence of particulate and dissolved materials was computed as $K_{bio} = K_d - K_w$ for 440 nm, where K_w is the coefficient for pure water equal to 0.00885 m^{-1} at 440 nm (Morel & Maritorena, 2001).

A hierarchical cluster analysis (HCA) was applied in order to classify the $R_{rs}(\lambda)$ spectra into coherent groups. The applicability of this method in the classification of hyperspectral $R_{rs}(\lambda)$ dataset for coastal waters was demonstrated by Lubac and Loisel (2007). Because the preliminary classification from HCA was greatly degraded by noise in the red range of several $R_{rs}(\lambda)$ spectra, only the range between 400 to 600 nm was considered. Prior to running the HCA, each $R_{rs}(\lambda)$ spectrum was normalized to its mean value computed on the basis of all spectral values between 400 and 600 nm. The normalized spectrum is denoted $nR_{rs}(\lambda)$.

2.6. Bio-optical algorithms evaluation

A comparison was carried out between the measured Chl*a* with values retrieved from three bio-optical empirical algorithms, OC2v6 and OC4v6 derived for SeaWiFS data and OC3v6 for MODIS/Aqua (http://oceancolor.gsfc.nasa.gov/REPROCESSING/R2009/ocv6), using in situ measurements of $R_{rs}(\lambda)$. Furthermore, a matchup analysis was performed comparing in situ and remote-sensed Chl*a* retrieved from the Garver–Siegel–Maritorena semi-analytical algorithm (GSM) and in situ and remote-sensed phytoplankton absorption coefficients estimated from the GSM (Maritorena et al., 2002) and QAA (Lee et al., 2002) semi-analytical algorithms. The statistical parameters used for these evaluations were the mean relative percentage difference, *RPD*, and the mean absolute percentage difference, *APD*. The definitions of *RPD* and *APD* are presented in Table 3. The coefficient of determination, R^2, slope, and intercept obtained from the regression analysis of the log-transformed in situ measured data and algorithm-derived were also considered for evaluation of the performance of the empirical and semi-analytical algorithms.

2.7. Matchup analysis

MODIS satellite/Aqua level 1A and ancillary data of ozone concentration and meteorological conditions (wind speed, oxygen concentration, water vapor and atmospheric pressure) were obtained from NASA's Distributed Active Archive Center (DAAC). Full resolution imagery of the local area coverage (LAC) for the PATEX 2 to PATEX 7 cruises was used to evaluate products derived from empirical and semi-analytical algorithms. The selected images were processed to level 2 (L2), and the following data products were obtained: the Chl*a* retrieved from empirical (OC2v6, OC3v6, OC4v6) and semi-analytical (GSM) algorithms, the phytoplankton absorption coefficient retrieved from GSM and QAA algorithms, and the ancillary information, such as the solar and sensor zenith angles and the L2 processing flags. The SeaWiFS Data Analysis System (SeaDAS) software version 6.4 was used to process data from level 1 and the product retrievals.

For comparison between the in situ data and satellite products and to minimize georeference errors, median values were computed for all products in a 3-by-3 pixel window centered on the locations of the oceanographic stations. Furthermore, the coefficient of variation (CV) was computed for the Chl*a* within each 3 by 3 window, and the retrieved value was excluded if CV > 0.2. This process was carried out to avoid strong variation from non-homogeneous regions within each window (Bailey & Werdell, 2006). For the temporal threshold coincidence between the satellite and in situ measurements, we considered a ± 3 h window around the satellite overpass, which follows the NASA's criterion (Bailey et al., 2000).

3. Results and discussion

The surface Chl*a* for all six PATEX cruises varied in a wide range from 0.10 to 18.87 mg m^{-3} with a mean value of 2.85 mg m^{-3}. The Chl*a* for MCF and BMCF varied from 0.08 to 24.05 mg m^{-3} and 0.08 to 12.03 mg m^{-3}, respectively. The frequency distribution of Chl*a* at the surface, MCF, and BMCF are shown in Fig. 2 (N = 176, 159 and 85). The variability in chlorophyll-*a* concentration was mainly associated with differences in time and geographical locations of sampling among the different cruises and the phytoplankton size structure (Ferreira et al., 2013).

3.1. Phytoplankton and particulate absorption and diffuse attenuation coefficients

Table 1 shows the absorption coefficients at 440 nm of particulate material, $a_p(440)$, and phytoplankton, $a_{ph}(440)$, and the contribution of phytoplankton to the particulate absorption, $a_{ph}(440) / a_p(440)$, for each cruise. The data include surface, MCF, and BMCF measurements. Non-algal absorption, $a_p(440) - a_{ph}(440)$, did not co-vary with Chl*a*, regardless of the sampled depth (not shown), and its contribution was relatively low during all cruises (average of 13%), even with the high variability in Chl*a*.

Phytoplankton was the dominant component of the particulate absorption (Table 1), with the lowest and highest average contributions during PATEX 3 (81%) and PATEX 4 (96%). These results suggest

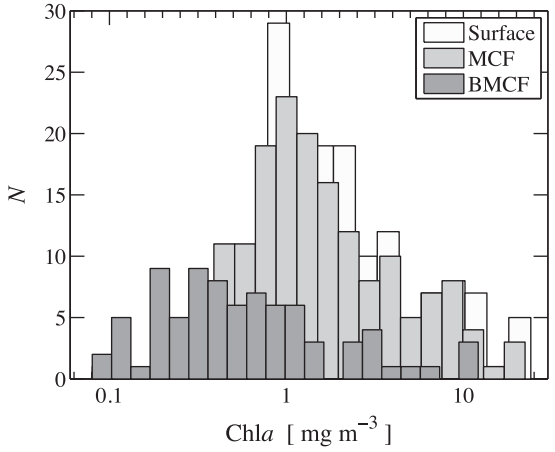

Fig. 2. Frequency histogram of the chlorophyll-*a* concentration, Chl*a*, measured at the near-surface (N = 176), the depths of maximum chlorophyll fluorescence, MCF (N = 159), and the base of maximum chlorophyll fluorescence, BMCF (N = 85), during the PATEX 2 to PATEX 7 cruises.

that for the shelf break and adjacent areas during the blooms in spring and summer, the particulate absorption is largely dominated by living cells and the relative proportions of detrital particulates shows little seasonal and interannual change. Our results on the percent contribution by phytoplankton are in agreement with the range of 85 to 94% found by Morel et al. (2006) for Case 1 waters with high chlorophyll concentrations.

Values of $a_p(440)$ ranged from 0.026 to 0.492 m^{-1} and increased (on a log scale) with increasing Chl*a* (0.08 to 24.02 mg m^{-3}) (Fig. 3a). Linear fitting between log-transformed data provided a R^2 of 0.77 ($N = 356$). Inferred from the general nonlinear character of this dependence (Bricaud et al., 1998) and the broad range of Chl*a* covered by our dataset, the chlorophyll-specific particle absorption, $a_p^*(440)$ ($a_p(440)$:Chl*a*) decreased with increasing Chl*a* and ranged widely from 0.023 to 0.237 m^2 mg^{-1}. The power function $a_p(440) = A\ \mathrm{Chl}a^B$, where the *A* and *B* parameters are derived from regression analysis, provided a reasonably good fit to our data and was comparable to previously derived average relationships (Bricaud et al., 1998; Morel et al., 2006). Our $a_p(440)$ values are on average 75% above the mean relationship of Bricaud et al. (1998), B98, whereas the positive departure from Morel et al. (2006) equation, M06, derived for Case 1 waters with high chlorophyll content averages only 19%. Therefore, our dataset deviated largely from the global "average relationship" (represented by B98 equation), while the difference is less marked if compared with an average relationship of eutrophic Case 1 waters (M06 equation). These differences have implications in bio-optical models in which the phytoplankton absorption is parameterized in terms of total chlorophyll-*a* concentration on the basis of average trends from other regions within the world's ocean.

The dependence of $K_{bio}(440)$ on Chl*a* is displayed in Fig. 3b, and a power law described this dependence in the same way as for $a_p(440)$. The lower R^2 (0.65) computed between Chl*a* and log-transformed $K_{bio}(440)$ was comparable to that for $a_p(440)$ and may be partially attributed to the lower number of $K_{bio}(\lambda)$ data, which comprises only surface samples ($N = 116$). We also compared our fitting relationship for Chl*a* and $K_{bio}(440)$ to the general prediction model recently re-analyzed by Morel et al. (2007), M07. The same systematically higher trend of our $a_p(440)$ compared to the general fittings (B98 and M06) was also verified for $K_{bio}(440)$ (Fig. 3b). On average, our $K_{bio}(440)$ was higher by approximately 26% to what was expected from M07. This finding is in agreement with $K_d(\lambda)$ being a rough proxy of the absorption coefficient, merging the dominant effect of absorption and to a lesser extent backscattering (Gordon, 1989), mainly when the phytoplankton is the dominant particulate component. Indeed, $K_{bio}(440)$ and $a_p(440)$ were linearly correlated (Fig. 3c) with a R^2 of 0.67. As expected, $K_{bio}(440)$ was higher than $a_p(440)$, as seen by the points above the 1:1 line, on average by 1.67-fold. It is important to note that the CDOM absorption increases exponentially towards blue and UV wavelengths, so its absorption contributes with an important amount to the diffuse attenuation at 440 nm. Although we could not quantify the effect of CDOM absorption on $K_{bio}(440)$, part of the variability in $K_{bio}(440)$ not explained by $a_p(440)$ may be attributed to CDOM absorption. The importance of CDOM in explaining part of the $K_{bio}(\lambda)$ variability towards lower wavelengths is emphasized by the lower R^2 (0.42) obtained between $K_{bio}(360)$ ($K_w(360)$ equal to 0.0216 m^{-1}, as provided by Morel and Maritorena (2001)) and $a_p(360)$. However, part of the dispersion for this dependence may be attributed to the correction procedure adopted for the β amplification factor, which is not optimized for computation of $a_p(\lambda)$ in the UV range.

Our previous work characterized the variability in the coefficients of phytoplankton absorption, $a_{ph}(\lambda)$, instead of $a_p(\lambda)$, as a function of Chl*a* for part of the data shown here (Ferreira et al., 2013). As inferred from the dominance of phytoplankton on particulate absorption showed in the present work, our $a_{ph}(\lambda)$ values were generally above the general relationships (Bricaud et al., 1995, 2004) for a given Chl*a*. Previous studies concluded that differing non-algal detrital material content for a given Chl*a* caused the systematic deviations from the average of particulate absorption vs. Chl*a* (e.g., Morel et al., 2007 and references therein). Our results for $a_p(\lambda)$ however, suggest that non-algal particles may not modify the relationship between the bulk optical properties and Chl*a*, which is generally used as a single index by traditional bio-optical models, but actually show that the dispersion between Chl*a* and $a_p(440)$ ($R^2 = 0.77$) is practically the same as for $a_{ph}(440)$ ($R^2 = 0.78$, Ferreira et al., 2013). Ferreira et al. also demonstrated that most of the variability in $a_{ph}(\lambda)$ as a function of Chl*a* was caused by variations in the dominant cell size of phytoplankton, according to a size factor retrieved from the $a_{ph}(\lambda)$ spectra. The systematic deviations in both $a_p(\lambda)$ and $K_{bio}(\lambda)$ as a function of Chl*a* for the Patagonia waters found compared to general trends can be therefore attributed to variations in the phytoplankton size.

3.2. Relationship between chlorophyll-a and particulate attenuation coefficient

At 660 nm, after deducting the attenuation by pure seawater, the particle attenuation coefficient is primarily (~97%, Loisel & Morel, 1998) caused by particle scattering. Fig. 4 shows $c_p(660)$ as a function of Chl*a* for the six PATEX cruises. Because the measurements of $c_p(660)$ were taken along the water column and Chl*a* concentrations data are from several discrete depths, a higher number of Chl*a* vs. $c_p(660)$ pairs were available ($N = 790$) than for $a_p(440)$ ($N = 356$). We compared our data to the relationship derived by Loisel and Morel (1998), LM98, for near-surface waters (their Eq. 5). We note that the LM98 relationship was established for a narrower Chl*a* range (0.2 to 3.0 mg m^{-3}), unlike the range of our dataset (0.08 to 24.05 mg m^{-3}). Our $c_p(660)$ data correspond to lower Chl*a* (PATEX 3, 6 and 7) and are in agreement with LM98 (Fig. 4). Conversely, Chl*a* and $c_p(660)$ pairs were considerably lower than LM98 for higher Chl*a* (PATEX 2 and 4).

Regarding the particulate absorption coefficients, a non-linear model described the dependence of $c_p(660)$ on Chl*a*, and a power function fit provided the relationship $c_p(660) = 0.343\ \mathrm{Chl}a^{0.37}$ for

Table 1
The mean, standard deviation (Std), and range of the absorption coefficient at 440 nm for particulates, $a_p(\lambda)$, and phytoplankton, $a_{ph}(\lambda)$, and the percent contribution of $a_{ph}(440)$ to $a_p(440)$ for each PATEX cruise. The data are means of pooled data from the near-surface, depths of maximum chlorophyll fluorescence, and the base of maximum chlorophyll fluorescence.

		PATEX 2 $N = 44$	PATEX 3 $N = 54$	PATEX 4 $N = 66$	PATEX 5 $N = 51$	PATEX 6 $N = 79$	PATEX 7 $N = 62$
$a_p(440)$	Mean	0.22	0.14	0.21	0.08	0.14	0.04
	Std	0.08	0.05	0.16	0.04	0.08	0.02
	Range	0.07–0.36	0.02–0.27	0.02–0.68	0.02–0.20	0.03–0.37	0.01–0.09
$a_{ph}(440)$	Mean	0.19	0.11	0.20	0.07	0.12	0.04
	Std	0.06	0.04	0.15	0.03	0.08	0.02
	Range	0.07–0.32	0.01–0.26	0.02–0.67	0.02–0.17	0.02–0.36	0.008–0.09
$a_{ph}(440)$ / $a_p(440)$	Mean	0.83	0.81	0.96	0.84	0.92	0.91
	Std	0.07	0.15	0.07	0.13	0.08	0.12
	Range	0.51–0.92	0.25–0.97	0.71–1.00	0.48–1.00	0.49–0.98	0.25–1.00

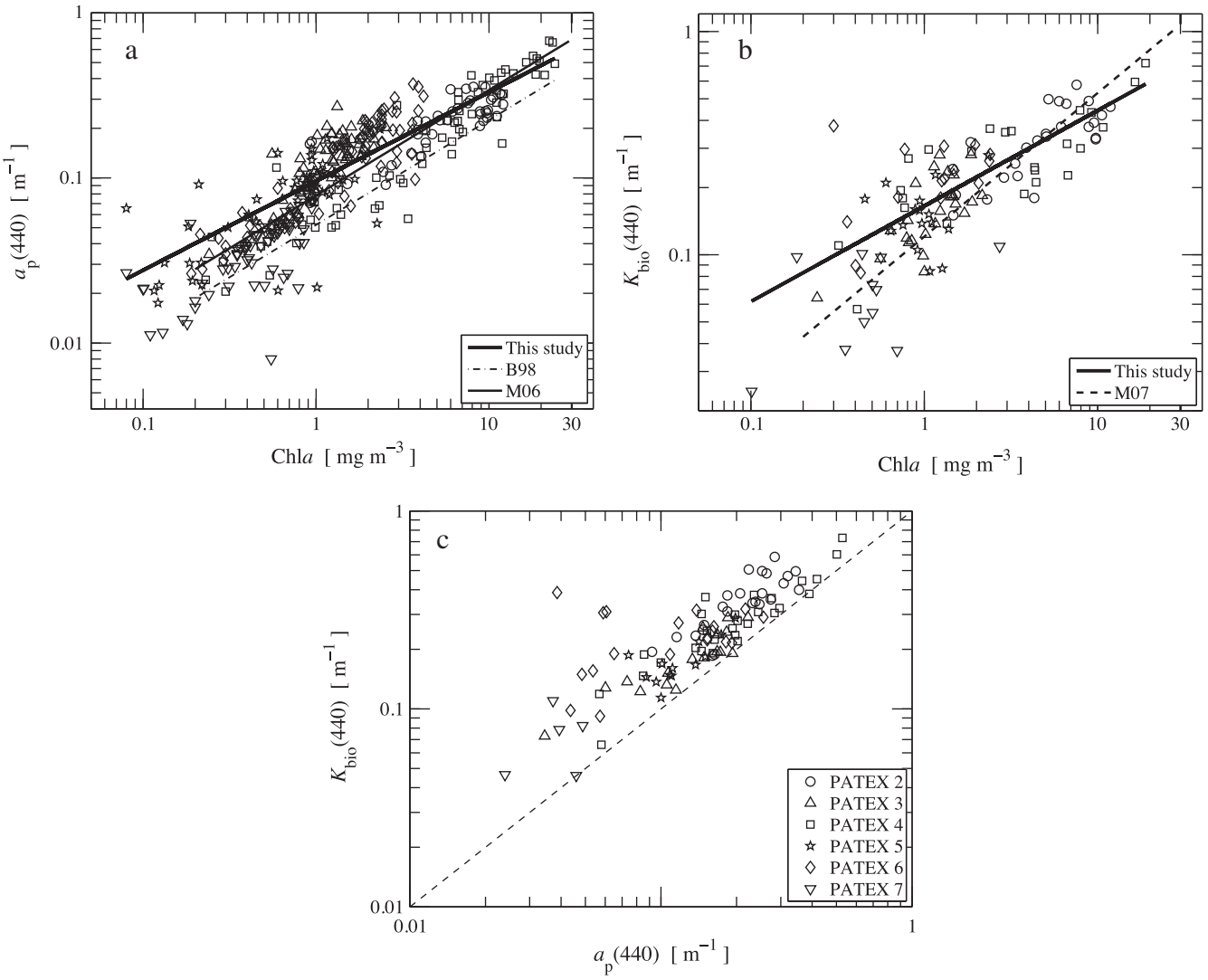

Fig. 3. (a) The particulate absorption coefficient at 440 nm, $a_p(440)$, as a function of chlorophyll-*a* concentration, Chl*a*, for near-surface depths, depths of maximum chlorophyll fluorescence and the base of the maximum depths during PATEX 2 to PATEX 7 cruises ($N = 356$, R^2 for log-transformed data = 0.77). As indicated, the lines represent the best fit regression between $a_p(\lambda)$ and Chl*a* ($a_p(440) = 0.096\ \text{Chl}a^{0.539}$) and lines B98 and M06 represent the previously derived relationships (Bricaud et al., 1998; Morel et al., 2006). (b) The diffuse attenuation coefficient at 440 nm, $K_d(440)$, as a function of Chl*a* for near-surface depths during PATEX 2 to PATEX 7 cruises ($N = 116$, R^2 for log-transformed data = 0.65). As indicated, the lines represent the best fit regression between $K_d(\lambda)$ and Chl*a* ($K_d(440) = 0.121\ \text{Chl}a^{0.644}$), and line M07 represents a previously derived relationship (Morel et al., 2007). (c) The diffuse attenuation coefficient at 440 nm, $K_d(440)$, as a function of $a_p(440)$ for near-surface depths during PATEX 2 to PATEX 7 cruises ($N = 116$, $R^2 = 0.67$). The dashed line represents a 1:1 ratio.

the entire dataset. Owing to the large dispersion of the data, the coefficient of determination obtained between the log-transformed data was relatively low ($R^2 = 0.60$, $N = 790$). The low exponent (0.37) indicates a deviation from linearity and relatively weak dependence. The high dispersion was partially associated with systematic differences between the cruises (Fig. 4), which was also observed for $a_p(440)$, although to a lesser extent (Fig. 3a). In general, higher values of $c_p(660)$:Chl*a* for a given Chl*a* were observed for PATEX 3, 6 and 7, and lower values for PATEX 2 and 4. Relatively high $c_p(660)$:Chl*a* ratios for PATEX 5 associated with a coccolithophorid bloom (Garcia et al., 2011) stand out from most of the data and were also more scattered. Therefore, a distinct fitting was applied to represent (i) PATEX 2 and 4 and (ii) PATEX 3, 6, and 7; (iii) PATEX 5 was considered separately.

Table 2 shows the power law equations resulting from the combination of all PATEX data and the data derived separately according to similar trends between cruises. The lowest coefficient *A* of the relationship obtained for PATEX 2 and 4 (0.254) indicates a lower relative magnitude of attenuation for a given Chl*a*, which indicates that the strong non-linearity (exponent = 0.471) may be explained by higher Chl*a* and large phytoplankton cells. The PATEX 3, 6, and 7 cruises, which showed relatively low Chl*a* in association with smaller-sized cells (Ferreira et al., 2013), revealed higher relative attenuation coefficients ($A = 0.333$) and a clear dependence on Chl*a* (exponent $B = 0.818$) tending to linearity ($c_p(660)$:Chl*a* nearly constant for all Chl*a* ranges). The highest coefficient *A* (0.610) and lowest exponent *B* (0.40) derived for PATEX 5 indicates relatively high attenuation values and a weak dependence on Chl*a* ($R^2 = 0.56$). This highlights the limitation of parameterizations for scattering (or backscattering) coefficients according to chlorophyll-*a* during coccolithophorid blooms because of the high scattering properties of the coccoliths ($CaCO_3$ platelets around cells) independent of Chl*a* (see Garcia et al., 2011). As expected, the generally weak dependence of $c_p(660)$ on Chl*a* for PATEX 5 is not verified for particulate absorption coefficients (Fig. 3a), which are specifically resultant from pigments.

Despite the variability around the mean in $c_p(660)$ as a function of Chl*a* (Loisel & Morel, 1998; this work) that was greater than the variability in $a_p(440)$, there was a general similarity in the variability

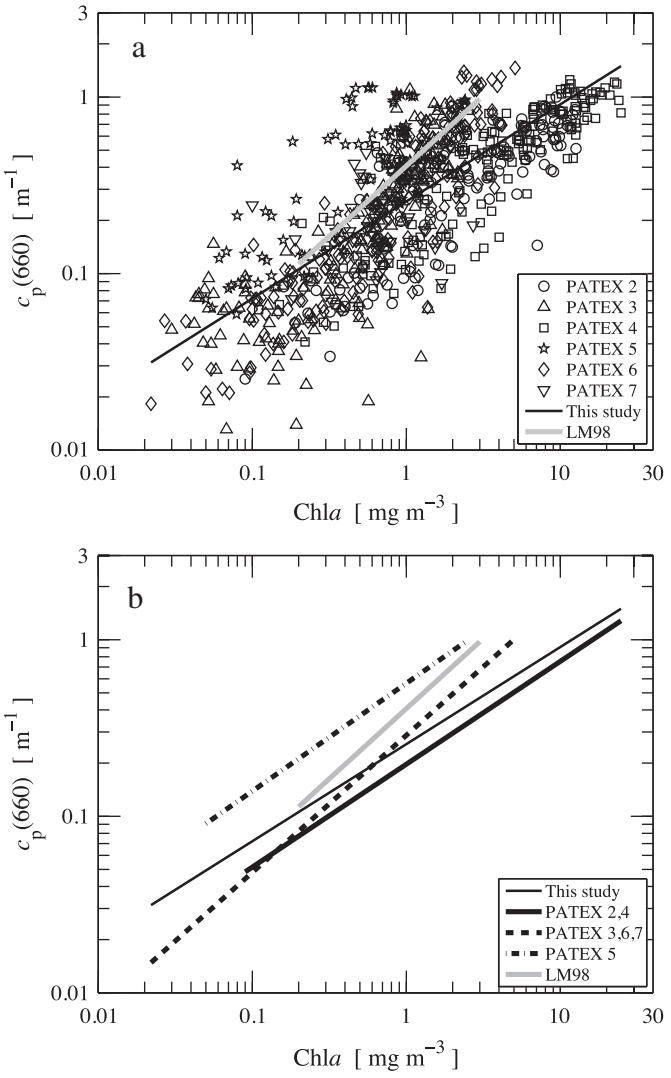

Fig. 4. (a) The particulate attenuation coefficient at 660 nm, $c_p(660)$, as a function of chlorophyll-*a* concentration, Chl*a*, for samples collected along the water column during the PATEX 2 through the PATEX 7 cruises ($N = 790$, R^2 for log-transformed data = 0.60). The line represents the best fit regression between $c_p(\lambda)$ and Chl*a* for the whole dataset. (b) The best fit regressions between $c_p(\lambda)$ and Chl*a* obtained for the whole dataset and separately according to cruises, as indicated (see Table 2). The previously derived relationship by Loisel and Morel (1998), LM98, derived for the Chl*a* range of 0.2 to 3.0 mg m^{-3} is shown in (a) and (b) for comparison.

of both coefficients (Figs. 3a and 4) caused by variations among the cruises. Our previous work (Ferreira et al., 2013) showed a strong relationship between the chlorophyll-specific particulate scattering coefficient at 660 nm, $b_p^*(660)$ ($b_p(660)$ normalized by Chl*a*) and the chlorophyll-specific phytoplankton absorption coefficient, $a_{ph}^*(440)$ ($a_{ph}(440)$ normalized by Chl*a*). Also, variations in chlorophyll-specific coefficients as a function of Chl*a* were mostly explained by differences in the phytoplankton cell size. In fact, Ferreira et al. (2013) derived two distinct power law relationships for $a_{ph}(440)$ as a function of Chl*a* by analyzing samples dominated by either nanophytoplankton or microphytoplankton.

Variations in $c_p(660)$ as a function of Chl*a* for Patagonia waters do not appear to reflect the physiological adjustments proposed by Behrenfeld and Boss (2003). Since the existing relationships between $c_p(\lambda)$ and phytoplankton biomass can be conceptually extended to use of particulate backscattering coefficients (Westberry et al., 2010), the variability in $c_p(660)$:Chl*a* presented here could be extended to applications of existing ocean color reflectance retrievals that depend on $b_b(\lambda) / a(\lambda)$. However, pronounced differences in scattering caused by a great variability in cell size structure associated with different stages of the bloom makes it difficult to establish a unique relationship between Chl*a* and scattering (or backscattering) for Patagonia waters.

Table 2
Results from regression analysis between the beam attenuation at 660 nm, $c_p(660)$, and the chlorophyll-*a* concentration, Chl*a*, for PATEX 2 to 7 cruises. The regression formula is $c_p(660) = A\ \mathrm{Chl}a^B$ where *A* and *B* are the best-fit parameters. The determination coefficient, R^2, and the number of data, *N*, are also shown. The results are presented for surface and selected depths based on the chlorophyll fluorescence profile. All regression analyses are significant for $p < 0.001$.

Cruise	Equation derived	R^2	*N*
All PATEX	$c_p(660) = 0.343\ \mathrm{Chl}a^{0.370}$	0.60	790
PATEX 2 and 4	$c_p(660) = 0.254\ \mathrm{Chl}a^{0.471}$	0.70	299
PATEX 3, 6 and 7	$c_p(660) = 0.333\ \mathrm{Chl}a^{0.818}$	0.70	397
PATEX 5	$c_p(660) = 0.610\ \mathrm{Chl}a^{0.400}$	0.56	94

3.3. Variability in the hyperspectral remote sensing reflectance spectra

The hyperspectral remote sensing reflectance spectra, $R_{rs}(\lambda)$, derived from the six PATEX cruises showed a great variability in both the magnitude and spectral shape (Fig. 5). The exclusion of the 600 to 700 nm range for the HCA (Section 2.5) eliminated the chlorophyll-*a* fluorescence peak centered at 683 nm, which was a conspicuous feature of several $R_{rs}(\lambda)$ spectra (Fig. 5). As expected, this peak was associated with $R_{rs}(\lambda)$ spectra in high Chl*a* samples. Three distinct classes were identified through a dendrogram and are illustrated in Fig. 6. The ordinary spectra, $R_{rs}(\lambda)$, for the three classes are also shown.

Class 1 covered the largest number of spectra ($N = 52$) and showed the highest $R_{rs}(\lambda)$ magnitudes among the three classes (Fig. 6a) and the greatest variability at lower wavelengths. The maximum reflectance was found at approximately 490 nm, and the magnitudes decreased towards higher wavelengths. Class 1 peaks corresponding to chlorophyll-*a* fluorescence at approximately 683 nm were not evident (not shown). Spectra with $R_{rs}(\lambda)$ higher than 0.01 sr^{-1} in the blue to the green wavelengths were found during the PATEX 5 cruise (Figs. 5d and 6a) and were associated with a great abundance of coccolithophorids (Garcia et al., 2011).

The $R_{rs}(\lambda)$ spectra of Class 2 and Class 3 were similar at the blue range and showed a concave shape between the main chlorophyll-*a* absorption band and the lowest reflectance at approximately 450 nm. The major differences between these classes were found in the green range, where Class 2 $R_{rs}(\lambda)$ spectra presented a wide peak between 490 and 560 nm, and Class 3 $R_{rs}(\lambda)$ spectra showed a distinct peak at 570 nm. Class 2 $R_{rs}(\lambda)$ spectra also showed a double peak in the green range of the spectrum with variable shapes ($N = 42$). Class 3 comprised the lowest number of spectra ($N = 22$), and except for two spectra with approximately 0.005 sr^{-1} close to 570 nm (Fig. 6e), the maximum absolute reflectance was always lower than 0.004 sr^{-1}. For both Class 2 and Class 3, the Chl*a* fluorescence emission peak near 683 nm can be seen (see Fig. 5).

The wide range of Chl*a* in the study region primarily explained the clustering identified through the HCA, with the lowest concentrations corresponding to Class 1 (mean 0.86 ± 0.51 mg m^{-3}) followed by intermediate concentrations in Class 2 (mean 2.42 ± 1.62 mg m^{-3}), and the highest concentrations in Class 3 (mean 8.40 ± 3.96 mg m^{-3}).

Class 1 contained few $R_{rs}(\lambda)$ spectra from PATEX 2, PATEX 4 and PATEX 6, most $R_{rs}(\lambda)$ spectra from PATEX 3, and all spectra from PATEX 5 and PATEX 7. Class 2 comprised the $R_{rs}(\lambda)$ spectra associated with moderate Chl*a* found in PATEX 2, the highest Chl*a* found in PATEX 3, the intermediate Chl*a* found in PATEX 4, the relatively high Chl*a* found in PATEX 6, and one $R_{rs}(\lambda)$ spectrum of PATEX 5.

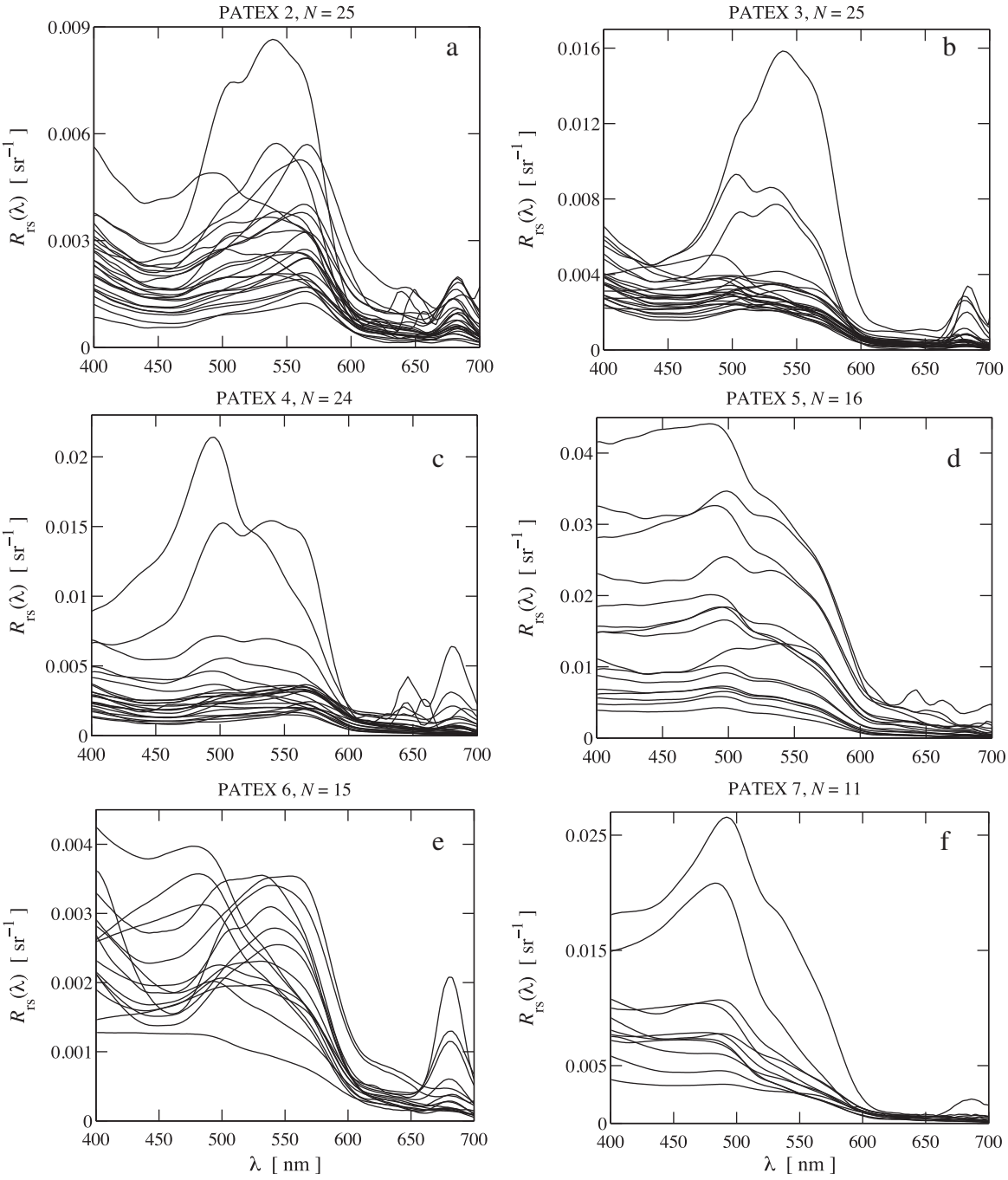

Fig. 5. Spectra of remote sensing reflectance, $R_{rs}(\lambda)$ in sr^{-1}, shown separately for (a) the PATEX 2 through the (b) PATEX 7 cruises. Note the different scales.

This spectrum was different from the other samples because, unlike other sites, diatoms were dominant (Garcia et al., 2011). Class 3 only included spectra from PATEX 2 and 4 (spring cruises). The environmental constraints and their effects on the distribution and temporal evolution of Chl*a* in the Patagonian Shelf-break have been discussed elsewhere on the basis of ocean color satellite data (Rivas et al., 2006; Romero et al., 2006) and physical and biological data collected during the PATEX cruises (Ferreira et al., 2013; Garcia et al., 2011; Souza et al., 2012).

Although no data for CDOM absorption is available, its contribution to the $R_{rs}(\lambda)$ spectra was probably minor because a noticeable decrease in $R_{rs}(\lambda)$ at the blue portion of the spectra and towards shorter wavelengths was not observed.

3.4. Evaluation of chlorophyll-a empirical algorithms

The analysis above showed that the $R_{rs}(\lambda)$ spectra from the Patagonia region may be separated according to spectral features that vary according to Chl*a*. In this section, we investigate the performance of operational empirical models that rely on the relationship between $R_{rs}(\lambda)$ band ratios and Chl*a*. Chl*a* was estimated from in situ $R_{rs}(\lambda)$ measurements from all cruises using the OC2v6, OC3v6 and OC4v6 empirical algorithms and compared to the in situ measured Chl*a*. Fig. 7 depicts the measured Chl*a* as a function of the $R_{rs}(\lambda)$ band ratios, relative to each of the three Chl*a* empirical algorithms, and their respective representational curves. The NOMAD dataset is also plotted as background for comparison.

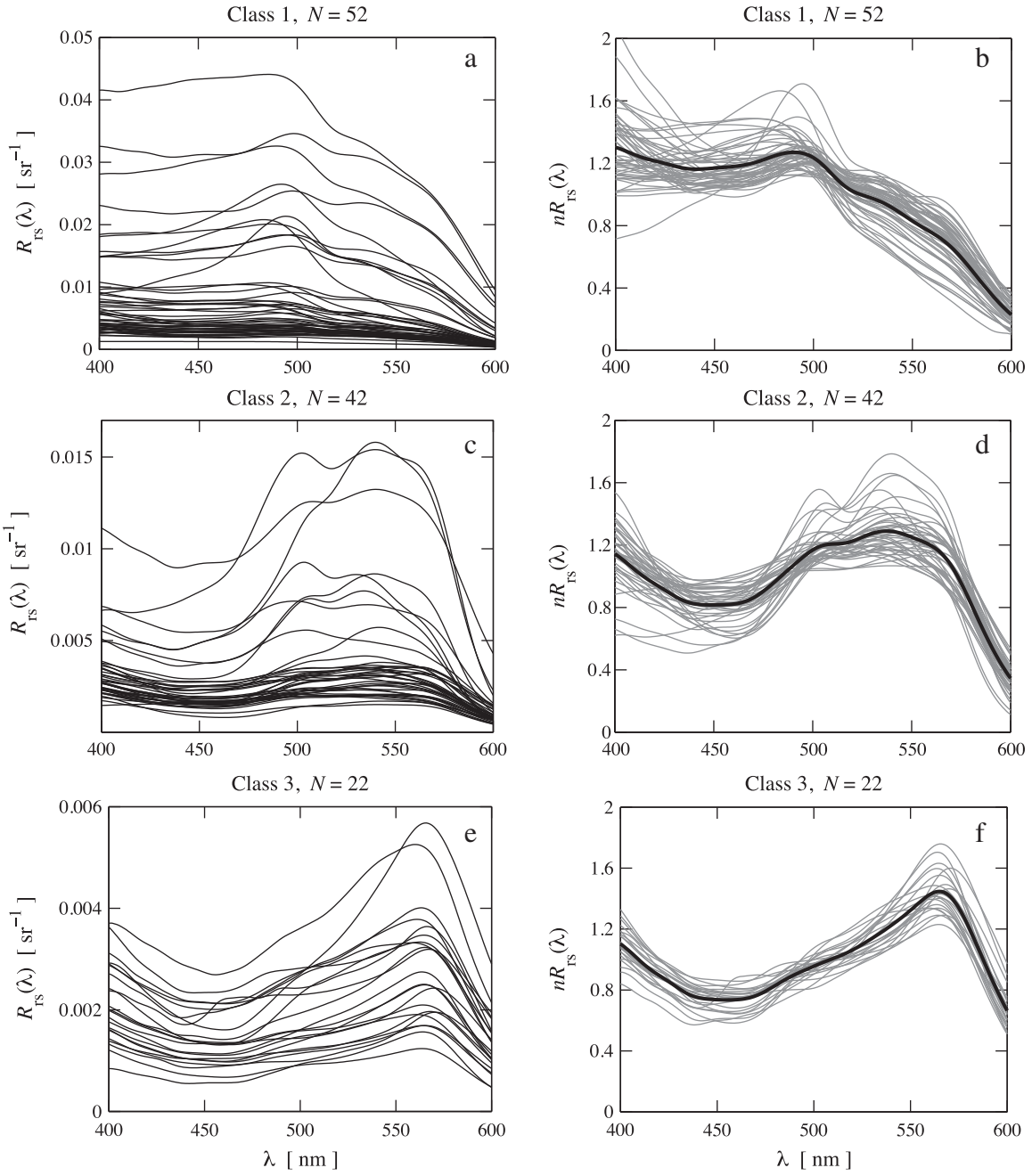

Fig. 6. Results of the hierarchical cluster analysis applied to the normalized remote sensing reflectance spectra, $nR_{rs}(\lambda)$. Both the absolute remote sensing reflectance, $R_{rs}(\lambda)$ in sr^{-1} (a, c, and e) and the $nR_{rs}(\lambda)$ with no unit (b, d, and f) are shown. The average $nR_{rs}(\lambda)$ spectra for each class are shown in bold.

Both the SeaWiFS 2-band (OC2v6) and MODIS 3-band (OC3v6) algorithms showed some deviation towards overestimating Chl*a* when considering the whole PATEX dataset (Fig. 7), with $R^2 = 0.67$ and 0.62, respectively, and a positive *RPD* (Table 3). The SeaWiFS 4-band (OC4v6) algorithm performed better ($R^2 = 0.78$) and had the lowest bias (*RPD* = 11.54%), and a mean absolute percentage difference (*APD* = 42.05%, Table 3). The results shown here are in agreement with previous analyses based on satellite data for the region (Dogliotti et al., 2009; Garcia et al., 2006).

In order to investigate whether the performance of chlorophyll empirical models are associated with variations in the spectral shape of $R_{rs}(\lambda)$ and variations in Chl*a*, the same empirical models used to retrieve Chl*a* were applied separately to each $R_{rs}(\lambda)$ class previously determined by HCA (Fig. 7). Linear fitting adjusted to measured and estimated log-transformed Chl*a* pairs were not statistically significant for most cases, which was probably due to the narrower Chl*a* range and the smaller dataset within each class. Thus, the performance of the models for each class was evaluated separately using R^2, slope, and intercept (Table 3). Regarding the OC4v6 algorithm, large errors (*RPD* = 31.80%; *APD* = 51.57%) were found for the class relative to moderate Chl*a* (Class 2), but there was a good agreement of the tested algorithm for the classes associated with the lowest (Class 1) and highest (Class 3) Chl*a* (*RPD* = −2.63% and *APD* = 30.82%; *RPD* = 6.30% and *APD* = 50.21%, respectively) (Table 3). Note that the poorer performance of the model for Class 2 was primarily explained by a narrower range of the estimated Chl*a* (0.97 to 4.69 mg m^{-3}), unlike the larger range found in the measured Chl*a* (0.74 to 7.96 mg m^{-3}). The performances of both the OC2v6 and OC3v6 algorithms were always poorer compared with the OC4v6 (Table 3 and Fig. 7).

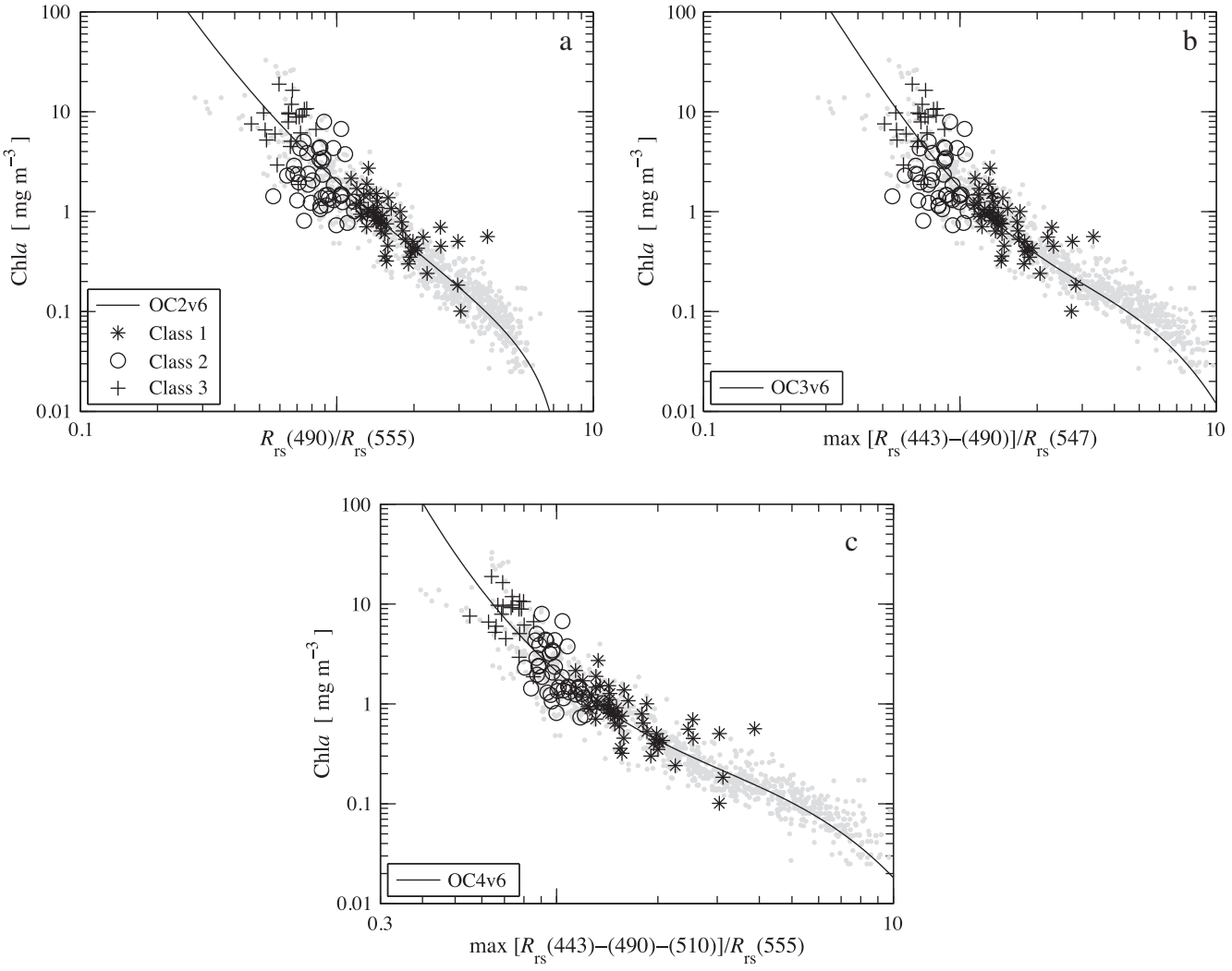

Fig. 7. Chlorophyll-*a* concentration, Chl*a*, as a function of the $R_{rs}(\lambda)$ band ratios used for the three Chl*a* empirical algorithms: (a) OC2v6, (b) OC3v6, and (c) OC4v6. The OC3v6 and OC4v6 algorithms use any of the two and three maximum (max) band ratios, respectively, as indicated on the *x* axes. The data are shown separately for the three $R_{rs}(\lambda)$ classes ordered by a hierarchical cluster analysis. The grey circles and solid curves represent NASA's Bio-optical Marine Algorithm Data Set (NOMAD) (Werdell & Bailey, 2005) and the indicated algorithms, respectively. Note that the axes have logarithmic scales.

Based on remote sensing reflectance, Moore et al. (2009) classified eight optical water types representative of the global ocean as determined from the NOMAD dataset. Although they verified a general pattern of increasing Chl*a* across the water types, the Chl*a* ranges overlapped between the types. The overlapping occurs in waters with the same chlorophyll-*a* content but distinct optical properties, such as suspended sediments and organic matter, pigment composition and cell size structure of phytoplankton. In our work, as the phytoplankton was shown to be the dominant particulate component and CDOM did not seem to play a noticeable role in determining the $R_{rs}(\lambda)$ spectra (Figs. 5 and 6), the overlap observed between the three classes in our data (Fig. 7) most likely reflects differences in phytoplankton optical properties for a given Chl*a*.

High relative errors are expected in the performance of empirical bio-optical models in high Chl*a* waters because of the increasing optical complexity from additional material besides phytoplankton in the eutrophic waters (Morel et al., 2006). Interestingly, the errors associated with Class 3 (high Chl*a*) were relatively low (Table 3). Thus, very high Chl*a* associated with phytoplankton blooms along the Patagonia Shelf break waters does not appear to result in large errors from empirical model performances. However, large errors were associated with intermediate to high Chl*a* (Class 2, Table 3). Although the CDOM contribution to the reflectance spectra appears to be low, its contribution to absorption should be properly assessed to determine how it might impact the empirical model's performance (e.g., Szeto et al., 2011).

3.5. Relations between empirical algorithm errors and inherent optical properties

Most of the empirical bio-optical algorithms used to derive Chl*a* rely upon relationships between the Chl*a* and the blue-to-green spectral ratios of $R_{rs}(\lambda)$. However, the shape and magnitude of the $R_{rs}(\lambda)$ spectra actually depend on backscattering and absorption coefficients (IOP), which reflect variations in the optical components of seawater. In this section, we investigate how the variations in the IOP in terms of normalization to Chl*a* might influence the performance of the chlorophyll-*a* empirical models applied to Patagonia in situ $R_{rs}(\lambda)$ data. As it is based solely on in situ radiometric and Chl*a* measurements, this analysis does not include any uncertainty attributed to atmospheric correction or satellite radiance accuracy. Only the OC4v6 model was considered in this analysis, because it performed best when applied to our dataset (Section 3.4). The relative error (*RE*) was defined as $RE = 100 * (\text{retrieved Chl}a - \text{measured Chl}a) / \text{measured Chl}a$.

Table 3
Statistical results for the performance of the three empirical algorithms, OC2v6, OC3v6, and OC4v6, to estimate the surface chlorophyll-*a* concentration, Chl*a*, from in situ $R_{rs}(\lambda)$ data collected during the PATEX 2 to PATEX 7 cruises. The algorithms were applied to all $R_{rs}(\lambda)$ data and separately to each of the three $R_{rs}(\lambda)$ classes obtained with a hierarchical cluster analysis. The mean relative percentage difference, *RPD*[a], and mean absolute percentage difference, *APD*[b], were computed between the measured Chl*a* and Chl*a* estimated from the algorithm. The R^2, slope and intercept derived from linear regression analysis on log-transformed measured and retrieved data were computed only when all $R_{rs}(\lambda)$ data were considered. The mean and standard deviation (Std) of surface Chl*a* corresponding to all $R_{rs}(\lambda)$ and to each $R_{rs}(\lambda)$ class are also shown (column 1).

Dataset Mean (Std)	Algorithm	*RPD*	*APD*	R^2	Slope	Intercept	*N*
All data	OC2v6	27.53	59.30	0.67	0.82	0.06	116
2.45 (3.42)	OC3v6	39.31	70.78	0.62	0.77	0.09	
	OC4v6	11.54	42.05	0.78	0.86	0.03	
Class 1	OC2v6	−2.93	29.95	–	–	–	22
0.86 (0.51)	OC3v6	1.82	31.84	–	–	–	
	OC4v6	−2.63	30.82	–	–	–	
Class 2	OC2v6	77.34	94.98	–	–	–	42
2.42 (1.62)	OC3v6	103.91	122.12	–	–	–	
	OC4v6	31.80	51.57	–	–	–	
Class 3	OC2v6	4.46	60.55	–	–	–	52
8.40 (3.96)	OC3v6	3.44	64.84	–	–	–	
	OC4v6	6.30	50.21	–	–	–	

X_{alg} and X_{meas} represent the algorithm-retrieved and measured values, respectively.

[a] $RPD = \sum_{n=1}^{N} \frac{X_{alg} - X_{meas}}{X_{meas}} \frac{1}{N} \times 100.$

[b] $APD = \sum_{n=1}^{N} \left| \frac{X_{alg} - X_{meas}}{X_{meas}} \right| \frac{1}{N} \times 100.$

Fig. 8 shows the dependence of relative errors of the OC4v6 algorithm-retrieved Chl*a* on the measured Chl*a* (Fig. 8a), $a_{ph}(440)$ (Fig. 8b), and $b_p(660)$ (Fig. 8c), both coefficients normalized by Chl*a* ($a_{ph}^*(440)$ and $b_p^*(660)$, respectively, in $m^2\ mg^{-1}$). $b_p(660)$ was computed as $c_p(660)$ subtracted $a_p(660)$.

The *RE* is scattered over the entire Chl*a* range (Fig. 8a), but significant relationships ($\alpha = 95\%$) were observed when each class was considered separately ($p < 0.001$ for Class 1, Class 2, and Class 3), and a general trend of underestimation emerged as Chl*a* increased. Likewise for Chl*a*, significant correlations were found between *RE* and $a_{ph}^*(440)$ ($p < 0.001$ for Class 1, Class 2, and Class 3) and $b_p^*(660)$ ($p = 0.02$ for Class 1 and $p < 0.0001$ for Class 2, and Class 3) and a clear tendency towards overestimation emerged for the retrieved Chl*a* according to increases in both $a_{ph}^*(440)$ and $b_p^*(660)$ (Fig. 8b and c).

Variations in $a_{ph}^*(\lambda)$ are associated with phytoplankton pigment packaging, which may be affected by variations in both the accessory pigments and cell size. Relatively lower Chl*a* and higher $a_{ph}^*(\lambda)$ are indicative of phytoplankton with small and lesser-packaged cells, whereas high Chl*a* and lower $a_{ph}^*(\lambda)$ are associated with large, highly packaged cells (Bricaud et al., 1995 and references therein). Our previous work (Ferreira et al., 2013) confirmed that variations in $a_{ph}^*(440)$ were related to cell size for the data presented here, indicating that most of the variability in phytoplankton absorption coefficients in Patagonia waters is explained by changes in the dominant cell size. Interestingly, the same trend was verified for $b_p^*(660)$, whereas a linear relationship held between $a_{ph}^*(440)$ and $b_p^*(660)$ (Ferreira et al., 2013). The direct dependence of *RE* on both $a_{ph}^*(440)$ and $b_p^*(660)$ shown here indicates that the empirical algorithm's uncertainties vary systematically with phytoplankton size structure.

The empirical algorithms assume that the sources of variability in $R_{rs}(\lambda)$ originate from Chl*a* and the covariation between the detrital (dissolved and particulate) component and Chl*a* (O'Reilly et al., 2000). Thus, variations in pigment packaging, species composition, and the abundance of colored detrital matter (CDM) relative to phytoplankton biomass lead to errors in the performance of empirical algorithms. The trend of increasing errors with increasing Chl*a*-specific phytoplankton absorption coefficients observed here was verified by Loisel et al. (2010) and Szeto et al. (2011) using the NOMAD global dataset, which covered a large, dynamic range that had systematic differences among the oceans with respect to $a_{ph}^*(\lambda)$ and CDM contribution (Szeto et al., 2011). It is interesting to note that regional and temporal differences associated with the phytoplankton blooms in Patagonia waters resulted in a Chl*a* range (0.10 to 18.87 mg m^{-3} at surface) wide enough to produce differences in Chl*a*-specific IOP and impact the Chl*a* retrieval from empirical models. The $b_p^*(660)$ was also shown to explain the OC4v6 algorithm errors. Although $R_{rs}(\lambda)$ depends on backscattering instead of scattering coefficients, the dependence of *RE* on $b_p^*(660)$ found here agrees with Westberry et al. (2010), who argued that variations in $b_p(\lambda)$ could be conceptually extended to particulate backscattering coefficients.

Our results clearly address the need to account for the influence of Chl*a*-specific IOP variability in Chl*a* retrieval algorithms for Patagonia waters. Regional parameterizations of semi-analytical ocean color algorithms with chlorophyll-specific IOP derived from the cluster analysis have the potential to improve product retrievals, as shown by Tilstone et al. (2012). Classification of the $R_{rs}(\lambda)$ spectra prior to application of specific bio-optical algorithms may also represent a valuable method of improving remote sensing retrievals (Lubac & Loisel, 2007; Moore et al., 2009).

3.6. Matchup analyses

Although semi-analytical ocean color models, which are based on the relationship between AOP and IOP (Gordon et al., 1988), have the potential to improve the retrieval estimates from remote sensing reflectance, some approximations have to be assumed. An empirical step of the QAA model (Lee et al., 2002) assumes spectral ratios of $R_{rs}(\lambda)$, whereas the GSM model (Maritorena et al., 2002) requires the assumption of mean spectral shapes for absorption and backscattering coefficients. In this section, we evaluated the performance of semi-analytical algorithms in retrieving phytoplankton absorption coefficients for Patagonia waters using models embedded in the SeaDAS software, that have fixed input parameters for the semi-analytical models.

Matchup analyses were performed to compare coincident in situ phytoplankton absorption coefficients with those estimated by the GSM and QAA semi-analytical models. We also compared in situ-measured Chl*a* with satellite-derived Chl*a* from the three empirical algorithms (OC2v6, OC4v6, and OC3v6) and the GSM semi-analytical model. The total number of in situ surface Chl*a* and $a_{ph}(\lambda)$ samples collected during the six cruises was 176 (see Fig. 2 for Chl*a*). Because of cloud cover and the application of NASA's selection criteria of the temporal window (±3 h), the matchup points were reduced to about 30 depending on the availability of satellite data provided by the algorithm.

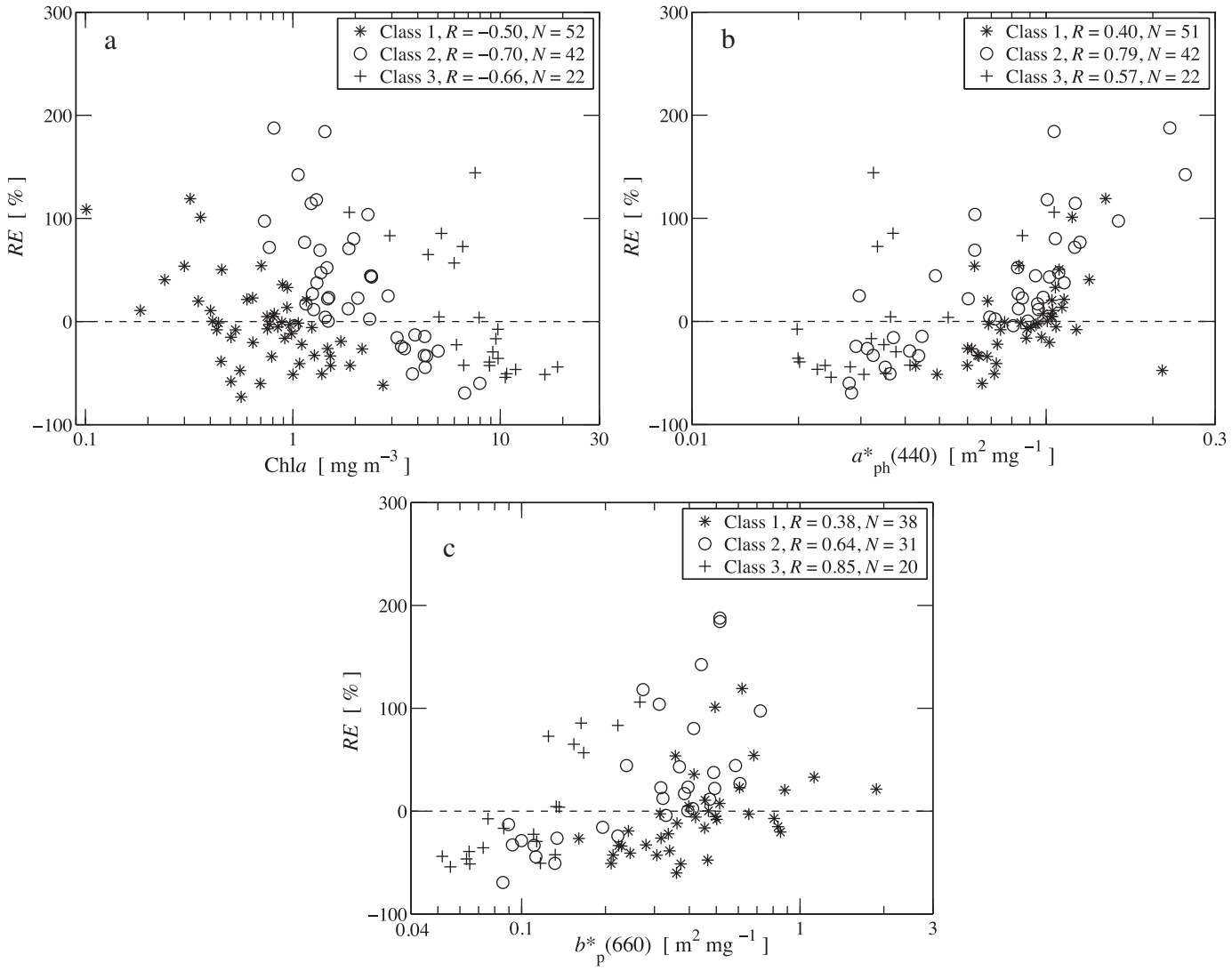

Fig. 8. Relative errors (*RE*) of the OC4v6 algorithm (see text for definition) as a function of (a) chlorophyll-*a* concentration, Chl*a*, (b) chlorophyll-specific absorption coefficient of phytoplankton at 440 nm, $a_{ph}^*(440)$, and (c) chlorophyll-specific scattering coefficient of particles at 660 nm, $b_p^*(660)$. The data are shown separately for the three $R_{rs}(\lambda)$ classes ordered by a hierarchical cluster analysis.

The matchup results are sorted by cruise instead of by $R_{rs}(\lambda)$ classes that was done for the retrievals using in situ $R_{rs}(\lambda)$ (Section 3.4), because of the reduced satellite data. Evaluation of the satellite model performance was made using the same statistics as in Section 3.4: R^2, slope, and the intercept between the log-transformed measured Chl*a* and satellite-estimated. The statistical evaluation of the algorithms is provided in each respective panel (Figs. 9 to 11).

Fig. 9 presents a comparison between the measured Chl*a* and algorithm-derived estimates. The dispersion between measured Chl*a* and satellite-estimated Chl*a* from empirical algorithms (Fig. 9a to c) was very similar to the dispersions using the in situ $R_{rs}(\lambda)$ dataset ($R^2 = 0.66$, 0.75 and 0.77 for OC2v6, OC3v6, and OC4v6, respectively). The major difference is that the estimates based on in situ $R_{rs}(\lambda)$ data tended to overestimate lower Chl*a* concentrations and underestimate higher Chl*a* concentrations, while the opposite was true for the satellite data (Fig. 9). This difference could be attributed to the discrepancy in the amount of data ($N \sim 33$ for matchup analysis against $N = 116$ for in situ dataset). Even so, there is a general trend of Chl*a* overestimation for both in situ and satellite $R_{rs}(\lambda)$ data, with *RPD* always positive (Table 3 and Fig. 9). The performance and overestimation of the GSM model is comparable to that of the empirical models (Fig. 9).

Scatter plots for satellite vs. measured $a_{ph}(\lambda)$ for blue and green wavelengths are shown in Figs. 10 and 11 as retrieved from the GSM and QAA algorithms, respectively. GSM underestimated $a_{ph}(412)$ with a strong negative bias ($RPD = -59\%$). Despite the general trend of underestimating lower $a_{ph}(\lambda)$ and overestimating higher $a_{ph}(\lambda)$ at other wavelengths, the GSM $a_{ph}(\lambda)$ at 469 and 488 nm corresponded reasonably to in situ data (Fig. 10). The errors for the green range of the spectrum, $a_{ph}(555)$, were larger ($R^2 = 0.47$ and $RPD = 181\%$, Fig. 10f) and the lowest dispersion between satellite and in situ data was achieved at 645 nm ($R^2 = 0.80$), although with the highest absolute and relative errors because of a considerable overestimation of the algorithm ($RPD = 90\%$ and $APD = 94\%$, not shown).

Errors in the estimates of $a_{ph}(\lambda)$ by GSM could result from differences between our values of the chlorophyll-specific phytoplankton absorption, $a_{ph}^*(\lambda)$, and the parameter $a_{ph}^*(\lambda)$ used in the algorithm. For instance, the mean value of $a_{ph}^*(\lambda)$ is assumed to be 0.0558 $m^2\ mg^{-1}$ at 443 nm (SeaDAS code). This value, however, can be highly variable in the field because of differences in algal cell size and pigment

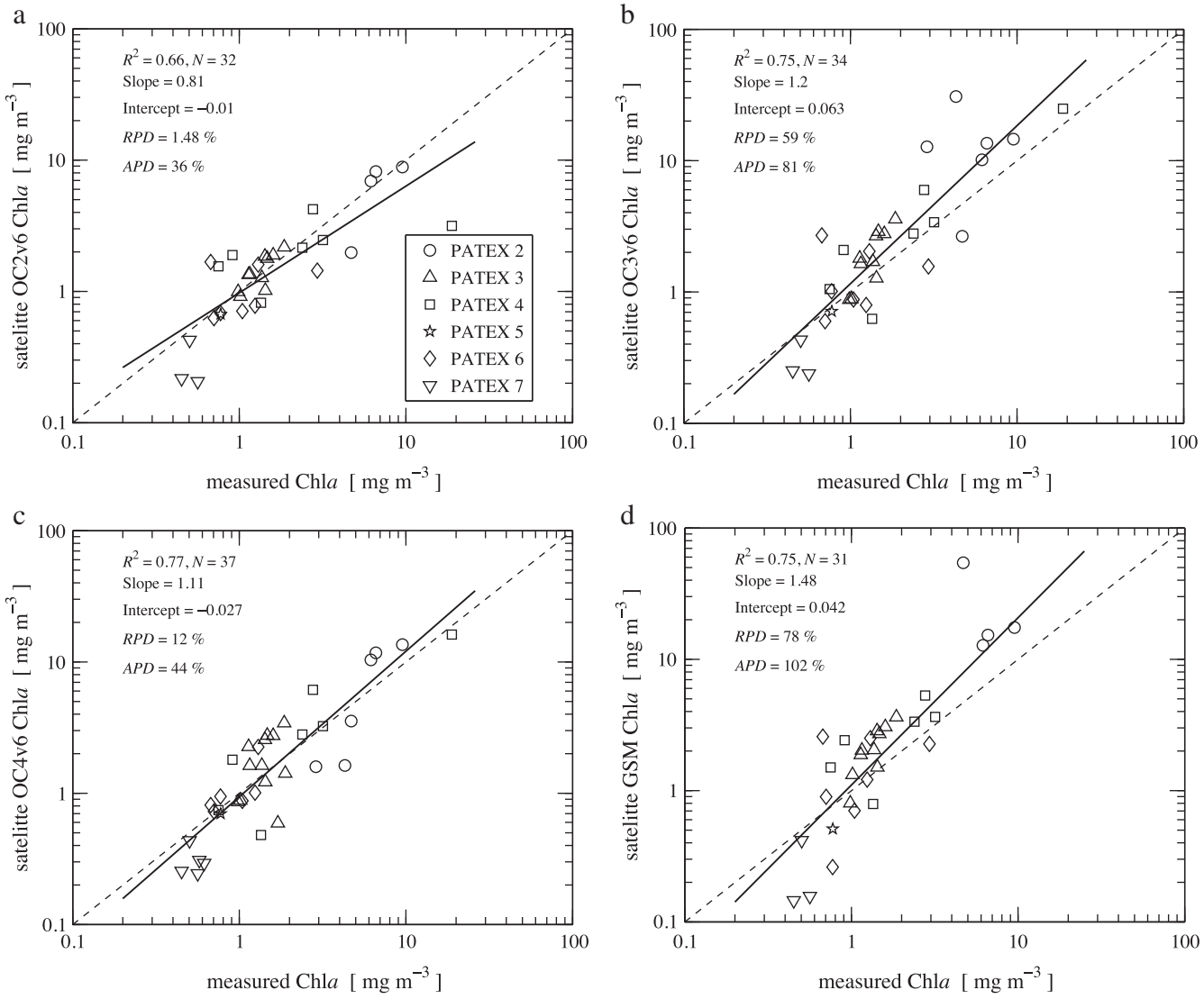

Fig. 9. Comparison between in situ-measured and satellite-retrieved chlorophyll-*a* concentration, Chl*a*, from the (a) OC2v6, (b) OC3v6, and (c) OC4v6 empirical algorithms, and the (d) GSM semi-analytical algorithm. Coefficient of determination, R^2, slope, and intercept obtained from regression analysis on log-transformed algorithm-derived and in situ measured data, the mean relative percentage difference, *RPD*, and mean absolute percentage difference, *APD*, are shown. The data are sorted by cruise.

composition. In our work, $a_{ph}^*(443)$ varied from 0.0180 to 0.2478 (average of 0.0721 m^2 mg^{-1}), which was generally higher than mean values used worldwide but it also varied seasonally (Ferreira et al., 2009, 2013). Higher values of $a_{ph}^*(\lambda)$ than the parameterization of the GSM algorithm would result in lower estimates of $a_{ph}(\lambda)$ and higher estimates of Chl*a*. Variability in magnitude and spectral variability of backscattering coefficients throughout the Patagonian region could also be cause of errors in the GSM estimates and deserves to be further studied.

In general, the QAA algorithm showed a better performance in retrieving $a_{ph}(\lambda)$, with points closer to the 1:1 line for 443, 469, 488, and 531 nm, compared to GSM-derived results. The highest agreement was observed at 488 nm with a *RPD* of −1.5% (Fig. 11c). The errors were substantially higher at 555 nm (*RPD* = 120% and *APD* = 132%), and the maximum disagreement between in situ and satellite data was observed at 645 nm (R^2 = 0.045) with a pronounced overestimation (*RPD* and *APD* = 509%, not shown). The better agreement between in situ and QAA satellite retrievals of $a_{ph}(\lambda)$ might result from the inexistence of spectral models of the absorption coefficients for this algorithm as for GSM.

4. Conclusions

In this study, a considerable variability was observed in the coefficients of particulate absorption, attenuation, and diffuse attenuation as a function of chlorophyll-*a* concentration, Chl*a*, in Patagonia waters during spring and summer phytoplankton blooms. This variability was shown to influence the performance of empirical models that derive Chl*a* from ratios of remote sensing reflectance. The errors in Chl*a* estimates by the empirical algorithm OC4v6 using in situ $R_{rs}(\lambda)$ showed significant statistical relationships with Chl*a*, $a_{ph}(440)$ / Chl*a*, and $b_p(660)$ / Chl*a*.

A hierarchical cluster analysis classified the hyperspectral $R_{rs}(\lambda)$ into three classes according to spectral features that corresponded to the variability in Chl*a*. This result indicates the dominant role of phytoplankton in controlling the optical properties of the spring and summer blooms along the Patagonia Shelf break region.

Although reasonable agreements were found between the measured and satellite-estimated Chl*a* and phytoplankton absorption coefficients, regional refinements of both empirical and semi-analytical algorithms that take into account the variability in Chl*a*-specific IOP

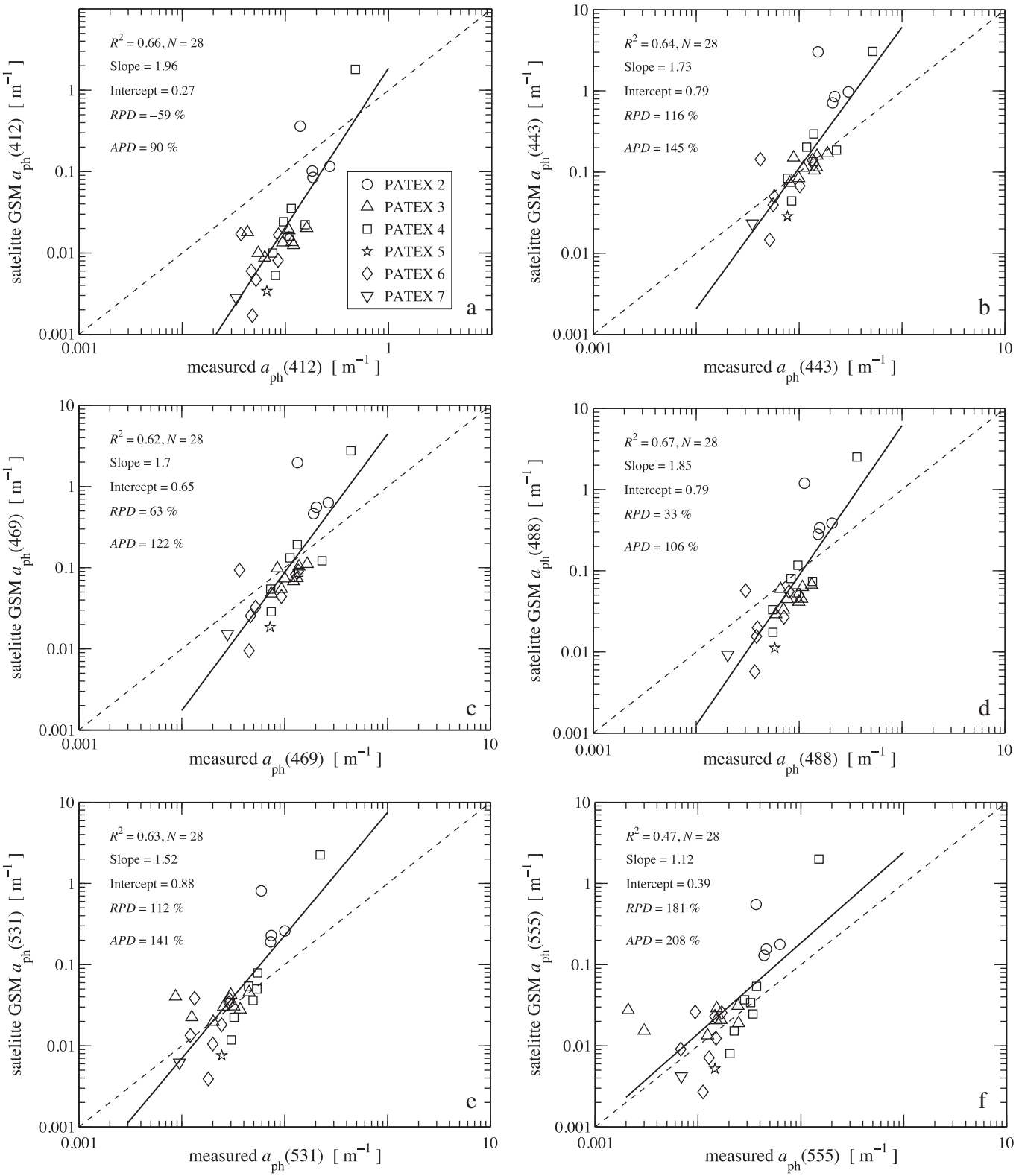

Fig. 10. Comparison between the in situ-measured and satellite-retrieved phytoplankton absorption coefficient, $a_{ph}(\lambda)$, from the GSM semi-analytical algorithm for blue and green wavelengths. The coefficient of determination, R^2, slope, and intercept obtained from regression analysis on log-transformed, algorithm-derived and in situ measured data, the mean relative percentage difference, *RPD*, and mean absolute percentage difference, *APD*, are shown. The data are sorted by cruise.

should improve the satellite estimates of the bio-optical properties for the Patagonia region. Our work contributed to the documentation of the bio-optical properties for high-Chl*a* waters, as recommended by Morel et al. (2006).

Acknowledgments

The PATagonian EXperiment (PATEX) is a multidisciplinary project conducted by the Group of High Latitude Oceanography (GOAL)

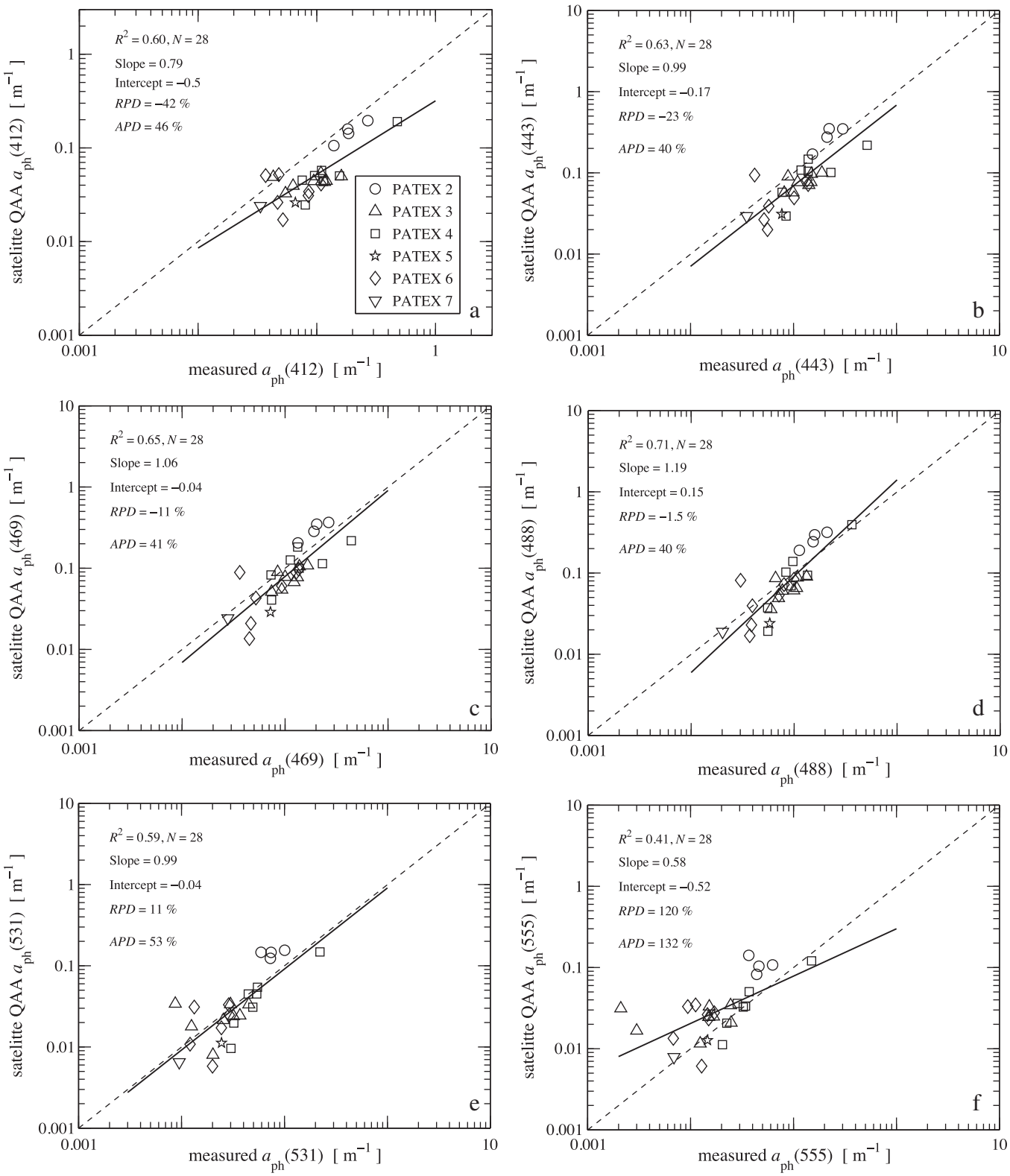

Fig. 11. Comparison between the in situ-measured and satellite-retrieved phytoplankton absorption coefficient, $a_{ph}(\lambda)$, from the QAA semi-analytical algorithm for blue and green wavelengths. The coefficient of determination, R^2, slope, and intercept obtained from regression analysis on log-transformed, algorithm-derived and in situ measured data, the mean relative percentage difference, *RPD*, and mean absolute percentage difference, *APD*, are shown. The data are sorted by cruise.

in the Brazilian Antarctic Program. We are grateful to the crew of the Brazilian Navy *R/V Ary Rongel* for their assistance during field experiments. We also acknowledge Servicio de Hidrografia Naval (Argentina) for their cooperation in obtaining clearance for carrying out the fieldwork within the Argentinean EEZ. The PATEX 5, 6 and 7 cruises were conducted as part of the Southern Ocean Studies for Understanding Climate Changes Issues (SOS-CLIMATE) project, a Brazilian contribution to the International Polar Year. The SOS-Climate project was funded by the Ministry of Science and Technology (MCT) and Brazilian National Council on Research and Development (CNPq, grant

520189/2006-0). This work was also partly supported by GSFC/NASA through the project OCEANS/04123400362 and by the NASA Biodiversity Program (Grant NNX09AK17G awarded to D.S.). A. Ferreira was funded by CNPq with a graduate scholarship (Proc. No. 143234/2008-0). We also thank two anonymous reviewers for their comments on the manuscript.

References

Aiken, J., Fishwick, J. R., Lavender, S., Barlow, R., Moore, G. F., Sessions, H., et al. (2006). Validation of MERIS reflectance and chlorophyll during the BENCAL cruise October, 2002: Preliminary validation of new demonstration products for phytoplankton functional types and photosynthetic parameters. *International Journal of Remote Sensing*, *28*, 497–516.

Arnone, R. A., Wood, A. M., & Gould, R. W., Jr. (2004). Water mass classification. *Oceanography*, *17*, 14–15.

Austin, R. W. (1974). The remote sensing of spectral radiance from below the ocean Surface. In N. G. Jerlov, & E. S. Nielsen (Eds.), *Optical aspects of oceanography* (pp. 317–344). La Jolla: Academic Press.

Bailey, S. W., McClain, C. R., Werdell, P. J., & Schieber, B. D. (2000). *Normalized water-leaving radiance and chlorophyll a match-up analyses*. NASA Tech. Memo. 206892, National Aeronautics and Space Administration, Goddard. Greenbelt, MD: Space Flight Center.

Bailey, S. W., & Werdell, P. J. (2006). A multi-sensor approach for the on-orbit validation of ocean color satellite data products. *Remote Sensing of Environment*, *102*, 12–23, http://dx.doi.org/10.1016/j.rse.2006.01.015.

Behrenfeld, M. J., & Boss, E. (2003). The beam attenuation to chlorophyll ratio: An optical index of phytoplankton photoacclimation in the surface ocean? *Deep Sea Research Part I*, *50*, 1537–1549, http://dx.doi.org/10.1016/j.dsr.2003.09.002.

Behrenfeld, M. J., & Boss, E. (2006). Beam attenuation and chlorophyll concentrations as alternative optical indices of phytoplankton biomass. *Journal of Marine Research*, *64*, 431–451, http://dx.doi.org/10.1357/002224006778189563.

Bianchi, A. A., Pino, D. R., Perlender, H. G. I., Osiroff, A. P., Segura, V., Lutz, V., et al. (2009). Annual balance and seasonal variability of sea–air CO_2 fluxes in the Patagonia Sea: Their relationship with fronts and chlorophyll distribution. *Journal of Geophysical Research*, *114*, C03018, http://dx.doi.org/10.1029/2008JC004854.

Bopp, L., Aumont, O., Cadule, P., Alvain, S., & Gehlen, M. (2005). Response of diatoms distribution to global warming and potential implications: A global model study. *Geophysical Research Letters*, *32*, L19606, http://dx.doi.org/10.1029/2005GL023653.

Brewin, R. J. W., Lavender, S. J., Hardman-Mountford, N. J., & Hirata, T. (2010). A spectral response approach for detecting dominant phytoplankton size class from satellite remote sensing. *Acta Oceanologica Sinica*, *29*(2), 14–32, http://dx.doi.org/10.1007/s13131-010-0018-y.

Bricaud, A., Babin, M., Morel, A., & Claustre, H. (1995). Variability in the chlorophyll-specific absorption coefficient of natural phytoplankton: Analysis and parameterization. *Journal of Geophysical Research*, *100*(C7), 13321–13332.

Bricaud, A., Claustre, H., Ras, J., & Oubelkheir, K. (2004). Natural variability of phytoplankton absorption in oceanic waters: Influence of the size structure of algal populations. *Journal of Geophysical Research*, *109*(C11), C11010, http://dx.doi.org/10.1029/2004JC002419.

Bricaud, A., Morel, A., Babin, M., Allali, K., & Claustre, H. (1998). Variations of light absorption by suspended particles with the chlorophyll a concentration in oceanic (Case 1) waters: Analysis and implications for bio-optical models. *Journal of Geophysical Research*, *103*(13), 31,033–31,044, http://dx.doi.org/10.1029/98JC02712.

Brown, C. A., Huot, Y., Werdell, P. J., Gentili, B., & Claustre, H. (2008). The origin and global distribution of second order variability in satellite ocean color and its potential applications to algorithm development. *Remote Sensing of Environment*, *112*, 4186–4203, http://dx.doi.org/10.1016/j.rse.2008.06.008.

Ciotti, A. M., & Bricaud, A. (2006). Retrievals of a size parameter for phytoplankton and spectral light absorption by Colored Detrital Matter from water-leaving radiances at SeaWiFS channels in a continental shelf region off Brazil. *Limnology and Oceanography Methods*, *4*, 237–253.

Ciotti, A. M., Lewis, M. R., & Cullen, J. J. (2002). Assessment of the relationships between dominant cell size in natural phytoplankton communities and the spectral shape of the absorption coefficient. *Limnology and Oceanography*, *47*(2), 404–417.

Dmitriev, E. V., Khomenko, G., Chami, M., Sokolov, A. A., Churilova, T. Y., & Korotaev, G. K. (2009). Parameterization of light absorption by components of seawater in optically complex coastal waters of the Crimea Peninsula (Black Sea). *Applied Optics*, *48*, 1249–1261.

Dogliotti, A. I., Schloss, I. R., Almanedoz, G. O., & Gagliardini, D. A. (2009). Evaluation of SeaWiFS and MODIS chlorophyll-a products in the Argentinean Patagonia Continental Shelf (38°S–55°S). *International Journal of Remote Sensing*, *30*, 251–273, http://dx.doi.org/10.1080/01431160802311133.

Ferreira, A., Garcia, V. M. T., & Garcia, C. A. E. (2009). Light absorption by phytoplankton non-algal particles and dissolved organic matter at the Patagonia Shelf-break in spring and summer. *Deep Sea Research Part I*, *56*, 2162–2174, http://dx.doi.org/10.1016/j.dsr.2009.08.002.

Ferreira, A., Stramski, D., Garcia, C. A. E., Garcia, V. M. T., Ciotti, Á. M., & Mendes, C. R. B. (2013). Variability in light absorption and scattering of phytoplankton in Patagonian waters: Role of community size structure and pigment composition. *Journal of Geophysical Research*, *118*, 698–714, http://dx.doi.org/10.1002/jgrc.20082.

Garcia, C. A. E., Garcia, V. M. T., Dogliotti, A. I., Ferreira, A., Romero, S. I., Mannino, A., et al. (2011). Environmental conditions and bio-optical signature of a coccolithophorid bloom in the Patagonia Shelf. *Journal of Geophysical Research*, *116*, C03025, http://dx.doi.org/10.1029/2010JC006595.

Garcia, V. M. T., Garcia, C. A. E., Mata, M. M., Pollery, R. C., Piola, A. R., Signorini, S. R., et al. (2008). Environmental factors controlling the phytoplankton blooms at the Patagonia Shelf-break in spring. *Deep Sea Research Part I*, *55*(9), 1150–1166, http://dx.doi.org/10.1016/j.dsr.2008.04.011.

Garcia, C. A. E., Sarma, Y. V. B., Mata, M. M., & Garcia, V. M. T. (2004). Chlorophyll variability and eddies in the Brazil–Malvinas Confluence region. *Deep Sea Research Part II*, *51*(1–3), 159–172, http://dx.doi.org/10.1016/j.dsr2.2003.07.016.

Garcia, V. M. T., Signorini, S., Garcia, C. A. E., & McClain, C. R. (2006). Empirical and semi-analytical chlorophyll algorithms in the Southwestern Atlantic coastal region (250–400 S and 600–450 W). *International Journal of Remote Sensing*, *27*(8), 1539–1562, http://dx.doi.org/10.1080/01431160500382857.

Gordon, H. R. (1989). Can the Lambert–Beer law be applied to the diffuse attenuation coefficient of ocean water? *Limnology and Oceanography*, *34*, 1389–1409.

Gordon, H. R., Brown, O. B., Evans, R. H., Brown, J. W., Smith, R. C., Baker, K. S., et al. (1988). A semianalytic radiance model of ocean color. *Journal of Geophysical Research*, *93*, 10909–10924.

Gregg, W. W., Casey, N. W., & McClain, C. R. (2005). Recent trends in global ocean chlorophyll. *Geophysical Research Letters*, *32*(3), L03606, http://dx.doi.org/10.1029/2004GL021808.

Gregg, W. W., Casey, N. W., O'Reilly, J. E., & Esaias, W. E. (2009). An empirical approach to ocean color data: Reducing bias and the need for post launch radiometric re-calibration. *Remote Sensing of Environment*, *113*, 1598–1612, http://dx.doi.org/10.1016/j.rse.2009.03.005.

Guidi, L., Stemmann, L., Jackson, G. A., Ibanez, F., Claustre, H., Legendre, L., et al. (2010). Effects of phytoplankton community on production, size, and export of large aggregates: A World-Ocean analysis. *Limnology and Oceanography*, *54*(6), 1951–1963.

Hirata, J. A., Aiken, J., Hardman-Mountford, N. J., Smyth, T. J., & Barlow, R. (2008). An absorption model to derive phytoplankton size classes from satellite ocean color. *Remote Sensing of Environment*, *112*, 3153–3159, http://dx.doi.org/10.1016/j.rse.2008.03.011.

http://oceancolor.gsfc.nasa.gov/REPROCESSING/R2009/ocv6/

http://www.wetlabs.com/cstar/

Huot, Y., Morel, A., Twardowski, M. S., Stramski, D., & Reynolds, R. A. (2008). Particle optical scattering along a chlorophyll gradient in the upper layer of the eastern South Pacific Ocean. *Biogeosciences*, *5*(2), 495–507.

International Ocean Colour Coordinating Group (IOCCG) (2006). Remote sensing of inherent optical properties: Fundamentals, tests of algorithms, and applications. In Z. P. Lee (Ed.), *IOCCG Rep. 5, Dartmouth, N. S., Canada*.

Kiørboe, T. (1993). Turbulence, phytoplankton cell size, and the structure of pelagic food webs. *Advances in Marine Biology*, *29*, 1–72.

Kirk, J. T. O. (1975). A theoretical analysis of the contribution of algal cells to the attenuation of light within natural waters. I. General treatment of suspensions of pigmented cells. *New Phytologist*, *75*, 11–20.

Kishino, M., Takahashi, N., Okami, N., & Ichimura, S. (1985). Estimation of the spectral absorption coefficients of phytoplankton in the sea. *Bulletin of Marine Science*, *37*(2), 634–642.

Le Quéré, C., Harrison, S. P., Prentice, C. I., Buitenhuis, E. T., Aumont, O., Bopp, L., et al. (2005). Ecosystem dynamics based on plankton functional types for global ocean biogeochemistry models. *Global Change Biology*, *11*, 2016–2040, http://dx.doi.org/10.1111/j.1365-2468.2005.01004.x.

Lee, Z. P., Arnone, R., Hu, C. M., Werdell, P. J., & Lubac, B. (2010). Uncertainties of optical parameters and their propagations in an analytical ocean color inversion algorithm. *Applied Optics*, *49*, 369–381.

Lee, Z. P., Carder, K. L., & Arnone, R. (2002). Deriving inherent optical properties from water color: A multi-band quasi-analytical algorithm for optically deep waters. *Applied Optics*, *41*, 5755–5772.

Loisel, H., Lubac, B., Dessailly, D., Duforer-Gaurier, L., & Vantrepotte, V. (2010). Effect of inherent optical properties variability on the chlorophyll retrieval from ocean color remote sensing: An in situ approach. *Optical Express*, *18*(20), 20,949–20,959, http://dx.doi.org/10.1364/OE.18.020949.

Loisel, H., & Morel, A. (1998). Light scattering and chlorophyll concentration in Case 1 waters: A reexamination. *Limnology and Oceanography*, *43*, 847–858, http://dx.doi.org/10.4319/lo.1998.43.5.0847.

Lubac, B., & Loisel, H. (2007). Variability and classification of remote sensing reflectance spectra in the eastern English Channel and southern North Sea. *Remote Sensing of Environment*, *110*, 45–58, http://dx.doi.org/10.1016/j.rse.2007.02.012.

Lutz, V. A., Segura, V., Dogliotti, A. I., Gagliardini, D. A., Bianchi, A. A., & Balestrini, C. F. (2010). Primary production in the Argentine Sea during spring estimated by field and satellite models. *Journal of Plankton Research*, *32*, 181–195, http://dx.doi.org/10.1093/plankt/fbp117.

Maritorena, S., Siegel, D. A., & Peterson, A. R. (2002). Optimization of a semianalytical ocean color model for global-scale applications. *Applied Optics*, *41*, 2705–2714.

Martinez-Vicente, V., Land, P. E., Tilstone, G. H., Widdicombe, C., & Fishwick, J. R. (2010). Particulate scattering and backscattering related to water constituents and seasonal changes in the Western English Channel. *Journal of Plankton Research*, *32*, 603–619, http://dx.doi.org/10.1093/plankt/fbq013.

Matano, R. P., & Palma, E. D. (2008). On the upwelling of downwelling currents. *Journal of Physical Oceanography*, *38*, 2482–2500, http://dx.doi.org/10.1175/2008JPO3783.1.

Mitchell, G. B., Bricaud, A., Carder, K., Cleveland, J., Ferrari, G., Gould, R., et al. (2000). Determination of spectral absorption coefficients of particles, dissolved material and phytoplankton for discrete water samples. *Ocean optics protocols for satellite ocean color sensor validation, Tech. Memo. 2000–209966* (pp. 125–153). Greenbelt, Md: NASA.

Mobley, C. D., Stramski, D., Bissett, W. P., & Boss, E. (2004). Optical modeling of ocean waters: Is the Case 1–Case 2 classification still useful? *Oceanography*, *17*, 60–67.

Moore, T. S., Campbell, J. W., & Dowell, M. D. (2009). A class-based approach to characterizing and mapping the uncertainty of the MODIS ocean chlorophyll product. *Remote Sensing of Environment*, *113*, 2424–2430, http://dx.doi.org/10.1016/j.rse.2009.07.016.

Morel, A. (1988). Optical modeling of the upper ocean in relation to its biogenous matter content (Case 1 water). *Journal of Geophysical Research*, *93*, 10,749–10,768.

Morel, A., Claustre, H., Antoine, D., & Gentili, B. (2007). Natural variability of bio-optical properties in Case 1 waters: Attenuation and reflectance within the visible and near-UV spectral domains, as observed in South Pacific and Mediterranean waters. *Biogeosciences*, *4*, 913–925.

Morel, A., Gentili, B., Chami, M., & Ras, D. J. (2006). Bio-optical properties of high chlorophyll Case 1 waters and of yellow-substance-dominated Case 2 waters. *Deep Sea Research Part I*, *53*, 1439–1459, http://dx.doi.org/10.1016/j.dsr.2006.07.007.

Morel, A., & Maritorena, S. (2001). Bio-optical properties of oceanic waters: A reappraisal. *Journal of Geophysical Research*, *106*, 7763–7780, http://dx.doi.org/10.1029/2000JC000319.

Morel, A., & Prieur, L. (1977). Analysis of variation in ocean color. *Limnology and Oceanography*, *22*, 709–722.

O'Reilly, J. E., Maritorena, S., Mitchell, B. G., Seigel, D. S., Carder, K. L., Garver, S. A., et al. (1998). Ocean color chlorophyll algorithms for SeaWiFS. *Journal of Geophysical Research*, *103*, 24937–24953.

O'Reilly, J. E., Maritorena, S., Siegel, D. A., O'Brien, M. C., Toole, D., Mitchell, B. G., et al. (2000). Ocean color chlorophyll a algorithms for SeaWiFS, OC2, and OC4: version 4. In S. B. Hooker, & E. R. Firestone (Eds.), *SeaWiFS postlaunch calibration and validation analyses, part 3.*, *Vol. 11.* (pp. 9–23). Greenbelt, Maryland: NASA, Goddard Space Flight Center.

Preisendorfer, R. W. (1961). Application of radiative transfer theory to light measurement in the sea. *International Union of Geodesy and Geophysics Monograph*, *10*, 11–30.

Rivas, A. L., Dogliotti, A. I., & Gagliardini, D. A. (2006). Seasonal variability in satellite measured surface chlorophyll in the Patagonia Shelf. *Continental Shelf Research*, *26*(6), 703–720, http://dx.doi.org/10.1016/j.csr.2006.01.013.

Romero, S. I., Piola, A. R., Charo, M., & Garcia, C. A. E. (2006). Chlorophyll-a variability off Patagonia based on SeaWiFS data. *Journal of Geophysical Research*, *111*, C05021, http://dx.doi.org/10.1029/2005JC003244.

Schloss, I. R., Ferreyra, G. A., Ferrario, M. E., Almandoz, G. O., Codina, R., Bianchi, A., et al. (2007). Role of plankton communities in sea–air variations in pCO_2 in the SW Atlantic Ocean. *Marine Ecology Progress Series*, *332*, 93–106, http://dx.doi.org/10.3354/meps332093.

Signorini, S., Garcia, V. M. T., Piola, A. R., Garcia, C. A. E., Mata, M. M., & McClain, C. R. (2006). Seasonal and interannual variability of calcite in the vicinity of the Patagonia Shelf Break (38°S–52°S). *Geophysical Research Letters*, *33*(16), L1, 6610, http://dx.doi.org/10.1029/2006GL026592.

Souza, M. S., Mendes, C. R. B., Garcia, V. M. T., Pollery, R., & Brotas, V. (2012). Phytoplankton community during a coccolithophorid bloom in the Patagonian Shelf: Microscopic and HPLC pigment analyzes. *Journal of the Marine Biological Association of the United Kingdom*, *92*, 13–27, http://dx.doi.org/10.1017/S0025315411000439.

Stramska, M., Stramski, D., Kaczmarek, S., Allison, D. B., & Schwarz, J. (2006). Seasonal and regional differentiation of bio-optical properties within the North Polar Atlantic. *Journal of Geophysical Research*, *111*(C8), C08003, http://dx.doi.org/10.1029/2005JC003293.

Szeto, M., Werdell, P. J., Moore, T. S., & Campbell, J. W. (2011). Are the world's oceans optically different? *Journal of Geophysical Research*, *116*, C00H04, http://dx.doi.org/10.1029/2011JC007230.

Tassan, S., & Ferrari, G. M. (1995). An alternative approach to absorption measurements of aquatic particles retained on filters. *Limnology and Oceanography*, *40*(8), 1358–1368.

Tilstone, G. H., Peters, S. W. M., van der Woerd, H. J., Eleveld, M. A., Ruddick, K., Schönfeld, W., et al. (2012). Variability in specific-absorption properties and their use in a semi-analytical Ocean Colour algorithm for MERIS in North Sea and Western English Channel coastal waters. *Remote Sensing of Environment*, *118*, 320–338, http://dx.doi.org/10.1016/j.rse.2011.11.019.

Voss, K. J. (1992). A spectral model of the beam attenuation coefficient in the ocean and coastal areas. *Limnology and Oceanography*, *37*(501–509), 1992.

Welschmeyer, N. A. (1994). Fluorometric analysis of chlorophyll-a in the presence of chlorophyll-b and pheopigments. *Limnology and Oceanography*, *39*(8), 1985–1992.

Werdell, P. J., & Bailey, S. W. (2005). An improved in situ bio-optical data set for ocean color algorithm development and satellite data product validation. *Remote Sensing of Environment*, *98*(1), 122–140, http://dx.doi.org/10.1016/j.rse.2005.07.001.

Westberry, T. K., Dall'Olmo, G., Boss, E., Behrenfeld, M. J., & Moutin, T. (2010). Coherence of particulate beam attenuation and backscattering coefficients in diverse open ocean environments. *Optical Express*, *18*(15), 15419–15425, http://dx.doi.org/10.1364/OE.18.015419.